3.18 MEMS Atomic Clocks

Svenja Knappe, National Institute of Standards and Technology (NIST), Boulder, CO, USA

Published by Elsevier B.V.

Glossary

AM Amplitude Modulation
ASIC Application-Specific Integrated Circuit
CAD Computer-Aided Design
CPT Coherent Population Trapping
CSAC Chip-Scale Atomic Clock
CSAM Chip-Scale Atomic Magnetometer
DBR Distributed Bragg Reflector
DFB Distributed Feedback
DRIE Deep Reactive Ion Etching
DRO Dielectric Resonator Oscillator
EIT Electromagnetically Induced Transparency
EOM Electro-Optical Modulator
FBAR Film Bulk Acoustic Resonator
FM Frequency Modulation
GNSS Global Navigation Satellite Systems (e.g., GPS, Galileo, Golnass)
HBAR High-tone Bulk Acoustic Resonator
ITO Indium Tin Oxide
KOH Potassium Hydroxide
LO Local Oscillator
MCXO Microprocessor-Controlled Crystal Oscillators
MEMS Microelectromechanical Systems
NEMS Nanoelectromechanical Systems
OCXO Oven-controlled Crystal Oscillator
STIRAP Stimulated Raman Adiabatic Passage
TCXO Temperature-Compensated Quartz Crystal Oscillators
UHV Ultra High Vacuum
VCO Voltage-Controlled Oscillator
VCSEL Vertical-Cavity Surface-Emitting Lasers

3.18.1 Introduction to MEMS Atomic Clocks

3.18.1.1 Introduction

Frequency references provide the base for a large number of applications such as digital communication, navigation systems, synchronization of networks, or power distribution. As the amount of data transferred increases and data rates become faster, more stringent requirements are placed on the timing systems. At the same time applications have become more mobile, increasing the demand for small low-power frequency references.

Atomic oscillators have provided the most stable frequency references for more than 50 years (Lyons 1950, Quinn 2005, Townes 1951). They provide unmatched frequency stability over long periods of time (from a few seconds to many years), because their resonance frequency is determined by the energy transition of the atoms – in contrast to crystal oscillators, where the resonance frequency is determined by the length of the crystal and is therefore much more susceptible to temperature changes, for example. But in order not to perturb the resonance frequency of the atoms and to probe it, often very complicated setups are required. Therefore, the large size, cost, and power consumption of most atomic clocks have restricted their use in real-world applications. Nevertheless, smaller versions of optically pumped rubidium standards (Bloch *et al.* 1993, Chantry *et al.* 1996, Ho *et al.* 1998, Koyama *et al.* 2000, McClelland *et al.* 1995, 1996, 1999, Rochat *et al.* 2002, Suzuki *et al.* 1998) with volumes around 100 cm^3 and power requirements of a few watts have become commercial standards. They are manufactured in the tens of thousands for use in cellular telecommunication networks (Kusters and Adams 1999). Space-qualified versions became critical members of the clock ensembles in Global Navigation Satellite Systems (GNSS). But a large number of portable in-field applications require smaller and less expensive frequency references with much lower power consumptions. Temperature-compensated quartz crystal oscillators (TCXOs) are small low-power, low-cost devices with relatively good performance over longer times, which have proven useful in such battery-operated portable applications. Nevertheless, their frequency stability at longer times (one hour to several days) is not sufficient for the requirements of many applications in the civil and military navigation and communication sector (Fruehauf 2001, Lee *et al.* 1996, Murphy and Skidmore 1994, Sturza 1984, Vig 1993). **Figure 1** summarizes typical performances of different commercially available oscillators as a function of averaging time (see Section 3.18.3.2 for an explanation of fractional frequency stability). It can be seen that crystal oscillators can be good frequency references over short times (see Section 3.18.2.3), but they are outperformed by atomic clocks at longer times.

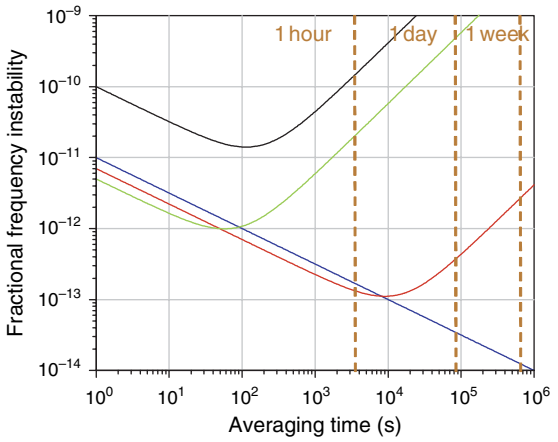

Figure 1 Typical performance of different commercially available oscillators: cesium beam standard (blue), rubidium vapor cell clock (red), oven-controlled crystal oscillator (OCXO, green), temperature-compensated crystal oscillator (TCXO, black).

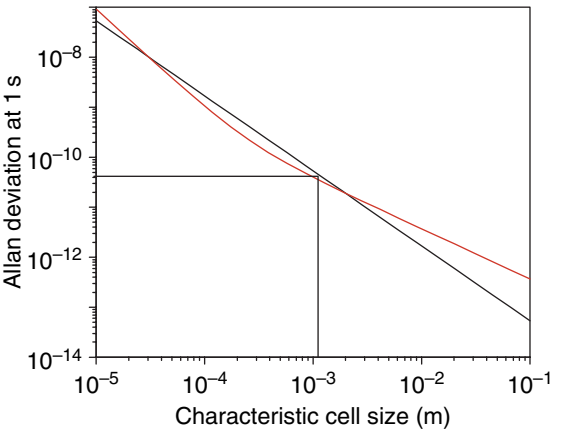

Figure 2 Estimate of the Allan deviation at 1 s as a function of characteristic cell size for a cell with a 100 kPa nitrogen buffer gas (red) or a paraffin wall coating (black).

Furthermore, it can be seen that atomic vapor cell clocks also have drifts over very long timescales (see Section 3.18.3.2.3).

The size of the optically pumped rubidium atomic frequency standards (RAFS) is largely limited by the size of the microwave cavity and the power goes mainly into heating the cell and the lamp. All-optical clocks were proposed years ago (Cyr *et al.* 1993, Levi *et al.* 1997), but the lack of reliable, low-noise, easy-to-use diode lasers at the atomic wavelengths have prevented their implementation into commercial clocks. When single-mode vertical-cavity surface-emitting laser (VCSEL) became available at 852 nm (the D_2 line of cesium) with large modulation bandwidths (King *et al.* 1998), their practicality for coherent population trapping (CPT) spectroscopy was demonstrated (Affolderbach *et al.* 2000). Soon after, the first miniature CPT clock prototype was demonstrated (Kitching *et al.* 2001a, Vanier *et al.* 2004). The idea to combine this CPT spectroscopy with fabrication methods developed for microelectromechanical systems (MEMS) into a chip-scale atomic clock (CSAC) was proposed (Kitching *et al.* 2002). MEMS fabrication techniques would allow for small size in an all-optical design and the use of a VCSEL in combination with small volume for correspondingly lower power requirements. An estimate of the fractional frequency instability of the clock stability at 1 s of integration as a function of cell size is shown in **Figure 2** for a 100-kPa N_2 buffer gas cell (red) and a paraffin wall coating (black) (Kitching *et al.* 2002). It can be seen that the fractional frequency stability of the clock degrades with smaller size, because of the more frequent collisions of the atoms with the cell walls. Nevertheless, stabilities below $1 \times 10^{-10}/\tau^{1/2}$ seem possible with a cell size of 1 mm (for an introduction to Allan deviation as a measure of frequency stability, see Section 3.18.3.2.1).

Since its proposal in 2002, the field of CSACs has rapidly progressed, largely due to the establishment of a CSAC program of the US Defense Advanced Research Projects Agency (DARPA). The goal of this program is to develop a MEMS atomic clock with a frequency instability of 1×10^{-11} at 1 h of integration in a package of volume 1 cm^3 consuming 30 mW of power. While this is still an ongoing project and the goals have not been reached yet, this chapter tries to outline some of the major developments so far. Since a majority of the work presented here was performed under the DARPA project with the goal of product development, many approaches cannot be reviewed here in detail, because no published information exists. Therefore, this review focuses mainly on MEMS clocks based on CPT, as most current approaches follow this route and a lot of published information exists. Nevertheless, other non-CPT approaches were successfully demonstrated and some of these are reviewed in Section 3.18.5.

3.18.1.2 Vapor Cell Atomic Clocks

The atoms in the gas phase are chosen for the best atomic clocks, because it is desirable to have distinct energy levels that are largely unperturbed by the

environment (as compared to the frequency bands of solids). The atoms in the first column of the periodic table, that is, alkali atoms, are favored in many atomic physics experiments because of their comparatively simple energy structure, determined largely by the single valence electron. The lowest energy electric dipole transitions in these atoms are called D-lines for historical reasons, and they correspond to changes in the distance between the valence electron and the nucleus, i.e., the transition $nS_{1/2} \leftrightarrow (n+1)P_{\mathcal{J}}$. The P state is split once again into two components of different total angular momentum $\mathcal{J}$ (**Figure 3(a)**). The atomic ground state ($S_{1/2}$) is split into two hyperfine energy components (F and F + 1), determined by the orientation of the electron spin relative to the spin of the nucleus. The clock frequency is determined by the energy difference between these hyperfine components divided by the Planck's constant h. Finally, the two hyperfine levels can be split into Zeeman sublevels in a magnetic field due to different orientations of the electron spin with respect to the magnetic field (m_F). Two of these Zeeman levels do not change their frequency to first order ($m_F = 0$ levels) in the presence of a magnetic field. These are usually chosen for the clock transition.

In an optically pumped vapor cell clock, one light field, e.g., with frequency ω_1, is present. It excites the atoms from state $|1\rangle$ into the excited state (**Figure 3(a)**). From there the atoms can decay into either of the two ground states. Eventually, a large fraction of atoms will accumulate in $|2\rangle$, a process called optical pumping (Happer 1972). The cell appears transparent because fewer atoms can absorb the light. When a microwave field with frequency $\omega_{\text{microwave}}$, equal to the clock transition frequency of the atom, is applied, the atoms can be repumped from $|2\rangle$ into $|1\rangle$. This microwave resonance can be detected through a change in the absorption of the light field.

Optical pumping in a RAFS, which are probably the most widely used atomic clocks in the world, is usually done with a rubidium discharge lamp (**Figure 3(b)**) (Vanier and Audoin 1989). It creates a broad spectrum of light, which is resonant with the transitions $5S_{1/2} \leftrightarrow 5P$. In order to enable efficient hyperfine pumping, the light needs to be spectrally filtered. This is done by using ^{85}Rb absorption, since the transition from one of the ground states in ^{85}Rb is very close to the one in ^{87}Rb. Therefore, RAFS usually have a ^{85}Rb filter cell in front of the ^{87}Rb clock cell (sometimes they are combined in the same cell though). After the filtered light passes through the ^{87}Rb cell, it is collected on a photodetector. A microwave cavity surrounds the ^{87}Rb cell to provide efficient coupling between the microwave field and the atoms and to ensure a uniform microwave phase over the entire volume of the cell. When the microwave frequency is exactly resonant with the atomic clock frequency of 6.8 GHz, the transmitted light decreases as atoms are pumped back into the depopulated hyperfine state. **Figure 3(c)** shows the transmitted light as a function of microwave frequency. Such a resonance can have Q factors of $\sim 10^8$.

RAFS can reach frequency stabilities in the range of 10^{-11} to $10^{-12}/\tau^{1/2}$ with centimeter cell sizes. At long times their frequency shows slow drifts around 10^{-14} per day; the detailed causes for this are still under investigation, but the diffusion of helium through the cell walls seems to be the one likely candidate

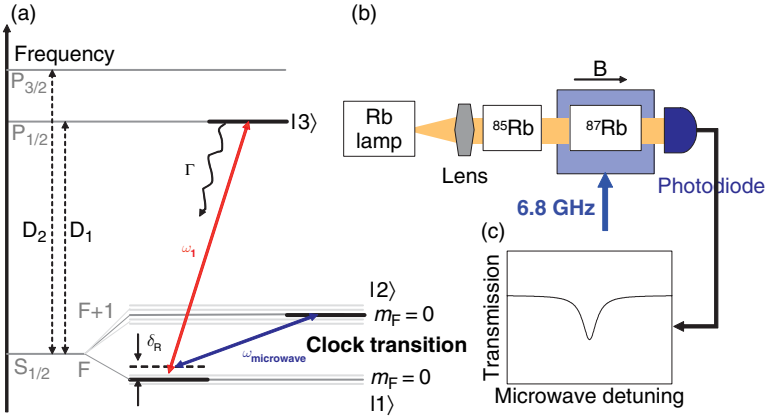

Figure 3 Schematic of the simplified atomic energy level configuration for the observation of (a) optically pumped microwave resonances, (b) spectroscopic setup, and (c) picture of a microwave resonance.

(Camparo 2004). The most power-consuming component in a RAFS is probably the Rb lamp. It has to be heated to high temperatures and usually consumes several hundred milliwatts to watts of power. The size of the RAFS physics package is largely determined by the size of the microwave cavity, since the clock frequency corresponds to ~4 cm. Therefore, it is challenging to miniaturize the current setup below the size of a deck of cards and to reduce the power consumption to below 1 W. In order to reduce the power consumption and the size of a vapor cell atomic clock, it would thus be useful to replace the lamp and the filter cell with a low-power laser and eliminate the microwave cavity.

3.18.1.3 Coherent Population Trapping

Heuristically, coherent population trapping (CPT) can be seen as a destructive quantum interference that happens, when the beat frequency between the two resonant light fields equals the ground state splitting frequency of the atoms. This destructive interference process largely reduces the probability that the atom can be excited by either of the light fields, so it appears dark, i.e., the resonance fluorescence is suppressed. CPT resonances have been studied for three decades. Alzetta *et al.* (1976) observed dark lines in the fluorescence emitted by a beam of sodium atoms. Simultaneously, the phenomenon was theoretically explained for a cascade system (Whitley and Stroud 1976) and for a Λ-System (Arimondo and Orriols 1976, Gray *et al.* 1978). Since then, the phenomenon of CPT and its related effect, electromagnetically induced transparency (EIT) (Fleischhauer *et al.* 2005, Harris 1997, Harris *et al.* 1990, Kasapi *et al.* 1995, Marangos 1998), have been suggested for a large number of applications such as optical bistability (Walls and Zoller 1980), laser cooling of atoms and ions (Aspect *et al.* 1988, Schmidt-Kaler *et al.* 2001), and lasing without inversion (Bentley Jr. and Liu 1999, Kocharovskaya 1992). The steep dispersion at CPT resonance at reduced absorption makes it attractive, for example, for the enhancement of nonlinear effects (Hemmer *et al.* 1995), slow light (Schmidt *et al.* 1996, Vestergaard Hau *et al.* 1999), optical data storage (Liu *et al.* 2001, Phillips *et al.* 2001), and gravitational wave detectors (Mueller *et al.* 1997). Finally, the narrow resonance linewidths (Brandt *et al.* 1997, Erhard *et al.* 2000, Merimaa *et al.* 2003) that can be achieved with CPT make it attractive for metrology applications (Tench *et al.* 1981, Thomas *et al.* 1982) where high-resolution laser spectroscopy can be applied to all-optical atomic clocks (Hemmer *et al.* 1983) and magnetometers (Bloom 1962, Scully and Fleischhauer 1992).

Although alkali atoms have a complicated structure of energy levels, the calculations for a simple system consisting of only three levels show surprisingly good agreement with the measurements (we will limit the introduction here to a very simplified picture for illustrative purposes only; for a review on CPT, see Arimondo 1996a). In these calculations, the so-called lambda system consists of two long-lived ground states $|1\rangle$ and $|2\rangle$, split by the clock frequency Δ_{HFS}, and an excited state $|3\rangle$ (**Figure 4(a)**, resembling the Greek letter Λ). Two light fields E_1 and E_2 with frequencies ω_1 and ω_2 and phases φ_1 and φ_2 can couple the electric dipole transitions $|1\rangle \leftrightarrow |3\rangle$ and $|2\rangle \leftrightarrow |3\rangle$. Both ground states have nearly equal populations in thermal

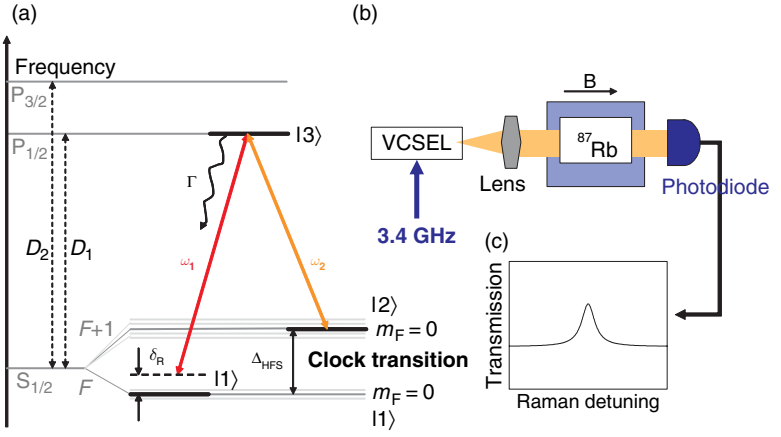

Figure 4 Schematic of the simplified atomic energy level configuration for the observation of (a) coherent population trapping (CPT) resonances (b) spectroscopic setup, and (c) picture of a CPT resonance.

equilibrium. A similar pumping as in microwave clocks can be performed between the ground states $|1\rangle$ and $|2\rangle$, when the two light fields E_1 and E_2 are resonant with the respective optical transitions (**Figure 4(a)**). If the beat frequency $\omega_1-\omega_2$ is equal to the clock frequency Δ_{HFS} then the atoms can be pumped into a so-called coherent dark state $|NC\rangle$.

For very simplified illustration purposes, we can choose a new basis $\{|C\rangle, |NC\rangle, |3\rangle\}$, where the coupled state $|C\rangle$ and the noncoupled state $|NC\rangle$ are superpositions of the atomic ground states (with notations from **Figure 4(a)**):

$$|C\rangle(t) \propto g_1|1\rangle + g_2 \exp(-i\Delta_{HFS}t + i\phi)|2\rangle \quad [1]$$

$$|NC\rangle(t) \propto g_2|1\rangle - g_1 \exp(-i\Delta_{HFS}t + i\phi)|2\rangle \quad [2]$$

Here, g_1 and g_2 are the so-called Rabi frequencies, which determine the interaction strength of the transition, and they are proportional to the amplitude of the respective light fields combined with atomic parameters. Furthermore, the time-dependent states have a frequency of Δ_{HFS} and a phase of ϕ. It can be shown that if the difference frequency between the light fields $\omega_1-\omega_2$ is equal to the ground-state splitting frequency Δ_{HFS}, and if the relative phase of the dark state ϕ is equal to the relative phase between the two light fields $\varphi_2-\varphi_1$, then the probability for an atom to be excited from $|NC\rangle$ by the light fields is zero.

In this case, a ground-state coherence is created that is out of phase with the beat between the driving light fields. The relative phase between the two light fields has to be stable in order for the state to remain dark and not to get an admixture of the coupled state $|C\rangle$. At the same time this places a constraint on the stability of the relative phase only (i.e., the microwave phase), and not on the individual phases of the light fields φ_1 and φ_2.

While this approach gives an intuitive explanation of the existence of a coherent dark state, it does not include the population of this state by spontaneous emission. It also fails to predict detailed lineshapes, dephasing, and decay rates. In order to include these effects, the density matrix approach has proven useful (Arimondo 1996b, Orriols 1979, Vanier *et al.* 1998)) for a three-level (Arimondo 1996a) or a four-level (Vanier *et al.* 2003c) system. When the Raman detuning $\delta_R = \omega_1-\omega_2-\Delta_{HFS}$ is scanned around zero, the CPT resonance is detected as a bright line in the transmission of the light fields (see **Figure 4(c)** for the transmission ($\sim$1 − absorption)). Many of the features of CPT resonances are similar to the ones of microwave resonances used in RAFS.

Again, the width of the CPT resonance is inversely proportional to the lifetime of the coherence. Since the decay times of the ground-state hyperfine levels are several thousand years for stable alkali atoms, the decoherence is determined by external factors such as collisions, magnetic field inhomogeneities, power broadening, and relative phase instability of the light fields.

To reduce the last broadening mechanism, two phase-stable optical light fields are used with a frequency splitting of a few gigahertz, which is tuned to match the ground-state hyperfine splitting of the atoms. This has been demonstrated by actively phase-locking (Enloe and Rodda 1965, Schmidt *et al.* 1996) two diode lasers, external modulation of one laser (Bouyer *et al.* 1996, Hemmer *et al.* 1983), injection locking of two lasers (Simpson *et al.* 2003), or direct modulation of the diode laser injection current (Cyr *et al.* 1993, Hemmer *et al.* 1993, Levi *et al.* 1997, Myatt *et al.* 1993, Stähler *et al.* 2002). While the first two methods are difficult to implement in a small low-power device for field applications that require ease of use and robustness, the last methods seem to be suitable for this. It requires lasers with large modulation bandwidths for most alkali atoms. Recently, distributed feedback (DFB) lasers have become available at Rb and Cs D_1 and D_2 lines with modulation bandwidths around 10 GHz. A simple and cheap technique was demonstrated by Affolderbach *et al.* (2000), using a single-mode VCSEL modulated at 9.2 GHz, in order to create sidebands for Cs CPT. Despite their broad linewidths of a few tens of megahertz, narrow CPT resonances have been measured. As has been emphasized before, the relative phase stability (given by the modulation) is more important to the CPT resonance than is the overall frequency stability of the light fields. The low operating power of VCSELs, their large modulation bandwidths, and vertical design make them well suited for small, low-power MEMS devices.

When miniaturizing an atomic clock, CPT systems seemed suitable, mainly because of the simplicity of the setup. It is challenging to reduce the size of a microwave cavity very much below the size of the associated microwave wavelength, e.g., 4 cm for ^{87}Rb. In contrast, there is no such size restriction for CPT, since the microwave frequency is carried through the beat frequency of the optical light fields (at least at sizes much larger than the optical wavelength). Since then, small microwave clocks have been demonstrated as well without the microwave cavities (see Section 3.18.5).

3.18.1.4 CPT in Small Vapor Cells

Extensive studies have compared the advantages and disadvantages of CPT over the microwave approach (Lutwak *et al.* 2002, Vanier *et al.* 2003e). Despite many similarities, there are substantial differences between the properties of CPT and optically pumped microwave resonances. First, in optically pumped clocks, a population imbalance must be created between the hyperfine levels. This is usually done by a single light field resonant with one of the transitions, which does not require phase coherence but makes the system more susceptible to light field-induced frequency shifts (Camparo *et al.* 1983, Mileti *et al.* 1998, Orriols 1979, Vanier *et al.* 1998). At the same time CPT resonances tend to have lower contrast than microwave resonances, because background light fields are often present and destructive interference between multiple excited states can exist.

Finally, since the microwave transition is created by a single photon of spin 1, only ground states with magnetic quantum numbers differing by $\Delta m = 0, \pm 1$ can be coupled. In CPT two light fields are used to couple the ground states, which allows for $\Delta m = 0$, ± 1, ± 2 (see Section 3.18.3.2.3.(i)).

In the following section, we consider what happens when the size of the vapor cell is reduced. For simplicity, we assume that all the three dimensions are equal to L. As we reduce the size of the cell, fewer atoms will be interrogated and less light will be absorbed. It has been found that the maximum CPT signal is obtained when roughly 50% of the light gets absorbed by the atoms (Godone *et al.* 2002, Knappe *et al.* 2002). In order to stay close to this optimum condition, the temperature, and thus the vapor pressure of the alkali atoms, needs to be increased for smaller cells.

A major contribution to the CPT linewidth are collisions of the alkali atoms with the cell walls. To reduce this effect, a buffer gas is added to the vapor cell, which increases the time for an alkali atom to reach the cell wall and eliminates residual Doppler broadening through Lamb–Dicke narrowing (Dicke 1953, Vanier and Audoin 1989). Usually, inert gases or molecules such as nitrogen or methane are used as buffer gases, because they have small cross sections σ_{puff} for the ground-state decoherence (Beverini *et al.* 1971). This causes a diffusive motion of the alkali atoms through the cell, and the CPT linewidth contributions can be approximated in the lowest-order diffusion mode by the following equation

$$\Delta \nu_{\text{CPT}}^{\text{diff}} \propto \frac{D_0}{L^2 p} \quad \text{and} \quad \Delta \nu_{\text{CPT}}^{\text{puff}} \propto \sigma_{\text{buff}}\, p \qquad [3]$$

for the diffusion and the buffer gas collision as a function of buffer gas pressure p. Here D_0 is the diffusion constant (see, e.g., Vanier and Audoin 1989, 1992 for values of D_0 and σ_{buff} and various alkali–buffer gas combinations). Thus, the linewidth is determined at low buffer gas pressures by the collisions of the alkali atoms with the cell walls, and at high pressures by collisions with the buffer gas atoms. It is a standard method to choose the buffer gas pressure to operate at the sweet spot of lowest linewidth (Beverini *et al.* 1971, Brandt *et al.* 1997) (**Figure 5**). It has been experimentally shown that the CPT resonance width agrees well with these predictions even at very small cell sizes of 100 µm (Knappe *et al.* 2004a). At the same time it means that when the operation is at the sweet spot, the linewidth increases with cell size like L^{-1} (Kitching *et al.* 2002).

CPT resonances have also been measured in large, but extremely thin cells with thicknesses below the optical wavelength without buffer gases (Sargsyan *et al.* 2006). This was done in a different regime, where the dimensions perpendicular to the laser beam had to remain large so that the linewidth was determined mainly by atoms with a small velocity component in the direction of the laser beam.

Although the buffer gases usually have a small depolarization cross section of the ground state, they cause substantial depolarization in the excited state, causing the P-state to broaden homogeneously at a few megahertz per kilopascal of pressure (Allard and Kielkopf 1982). If the excited-state decoherence rate Γ increases, more laser intensity is required to obtain the same amplitude and linewidth of the CPT resonance.

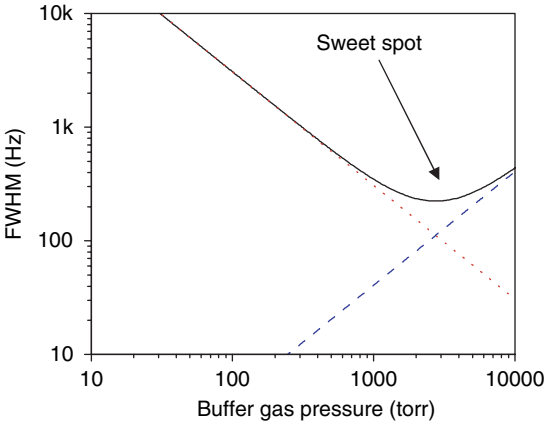

Figure 5 Coherent population trapping (CPT) linewidth as a function of buffer gas pressure in a 1-mm^3 cell filled with ^{87}Rb and N_2 as a result of diffusion to the walls (red dotted line), buffer gas collisions (dashed blue line), and the sum of both (black line).

At the same time, the absorption cross section of the atoms decreases so that the alkali vapor pressure, i.e., cell temperature, is increased to maintain a constant absorption. With an increase in alkali density, the rate of alkali–alkali spin-exchange collisions increases (Beverini *et al.* 1971, Happer 1972), i.e., rate is proportional to the alkali density. At sufficiently high pressures, spin-exchange collisions add a major contribution to the linewidth, rising proportional to the buffer gas pressure. In most vapor cells a molecular buffer gas, e.g., nitrogen, is included to quench the spontaneous emission and prevent radiation trapping (Copley and Krause 1969, Kibble *et al.* 1967).

Finally, the broadening of the excited state puts another constraint on very small CPT clocks. Since the bichromatic light field is usually produced by frequency-modulating a VCSEL at half the ground-state hyperfine frequency, the contrast of the CPT resonance is drastically reduced if the optical linewidth approaches the ground-state splitting frequency (Arimondo 1996a, Nikonov *et al.* 1994, Post *et al.* 2005). At these pressures the carrier and the second-order sidebands become resonant and can cause single-photon transitions out of the dark state (**Figure 6**). Furthermore, the beat frequency between the two first-order sidebands is out of phase with the ones between the carrier and the second-order sidebands. Since both beats have the same frequency, they could create dark states in the atoms, but with $\varphi_1 - \varphi_2$ having a difference of π, they cannot be dark simultaneously (eqns [1] and [2]). The phase relationships between the sidebands are symbolized in **Figure 6** by the direction of the arrows. Both effects reduce the lifetime of the coherence and degrade the stability of the clock.

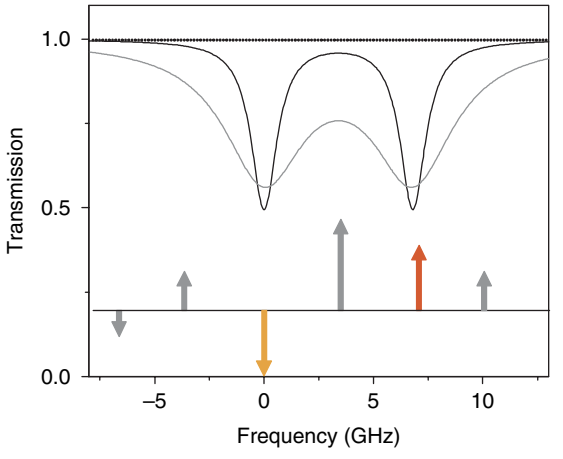

Figure 6 Transmission as a function of laser frequency relative to the transition of an atom with two ground states split by 6.8 GHz without buffer gas (black) and with homogeneously broadened lines (gray). The bottom arrows represent the sidebands created when the laser is modulated at 3.4 GHz and tuned such that the first-order sidebands (red and orange) are in resonance with the two atomic transitions. The direction of the arrows symbolizes the relative phase between them.

When frequency modulation (FM) of the VCSEL current is used, this places an upper limit on the buffer gas pressure. Thus, it is not necessarily favorable to operate at the sweet spot. The various parametric dependencies of the CPT clock resonance signals with cell parameters (such as buffer gas pressure, cell temperature, laser intensity, optical detuning, modulation frequency, and amplitude) have been characterized in detail (Knappe 2001, Knappe *et al.* 2001, Vanier 2001).

3.18.2 Design and Fabrication

3.18.2.1 Introduction

Passive CASCs in their simplest form consist of three parts: a local oscillator (LO) that generates the clock signal, a physics package that compares the frequency of the LO to the internal frequency of the atoms and outputs information about the difference frequency, and control electronics that tune the LO frequency such that the difference frequency is zero. Most CSACs use Cs or ^{87}Rb in their vapor cells, because of their relatively high ground-state splitting frequency (good Q factors), the availability of VCSELs at the right wavelengths, and relatively low vapor pressures.

In CPT-based CSACs, the LO usually produces a signal at half the ground-state hyperfine frequency of these atoms and modulates the injection current of a VCSEL. The frequency of the VCSEL is then tuned such that the two first-order modulation sidebands are in resonance with the two transitions from the ground-state hyperfine components to the excited state. Often, the buffer gas pressure is chosen to be above 5 kPa, so that the excited-state hyperfine structure is unresolved. The light is circularly polarized, attenuated, and sent through the alkali vapor cell. A photodiode detects the transmitted light. A small magnetic field parallel to the laser beam is applied to lift the degeneracy of the ground-state Zeeman levels and the cell is placed inside a magnetic shield to ensure a constant magnetic field strength. A schematic of this simple setup is depicted in **Figure 7**.

When the LO frequency is tuned to exactly half the ground-state frequency between the $m_F = 0$

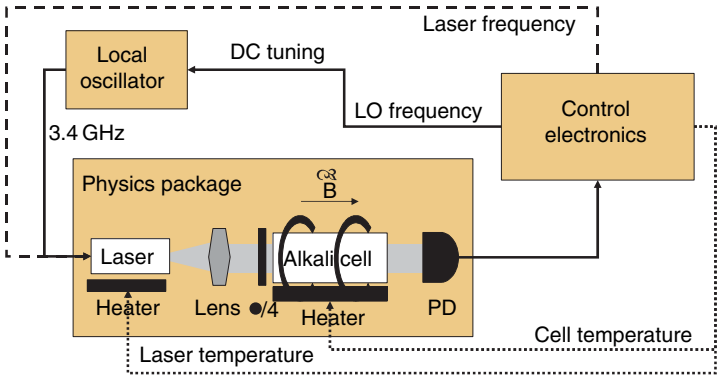

Figure 7 Schematic of a chip-scale atomic clock (CSAC) consisting of a local oscillator (LO), a physics package, and control electronics. The physics package consists of a laser with heater, lens, a quarter waveplate ($\lambda/4$), a vapor cell with heater, a magnetic offset field (B), and a photodetector (PD). The control electronics consist of servo loops for laser and cell temperature, as well as laser and LO frequency.

Zeeman components, the atoms are pumped into a coherent dark state and the transmitted light is reduced. To stabilize the LO frequency onto the top of the CPT resonance, its frequency is modulated at a few kilohertz. Phase-sensitive detection of the transmitted light at this frequency produces a dispersive error signal that can be used to lock the LO to the atomic resonance. A similar technique of phase-sensitive detection is used to lock the laser wavelength onto the center of the optical absorption by modulating the laser current at a low frequency. It is important that both of these modulation frequencies used for locking are well separated to avoid cross-talk between both loops. In addition to the two frequency-lock loops, two temperature servo loops are required to stabilize cell and laser temperatures. In some designs, the laser and the cell are in good thermal contact and one of the four feedback loops is eliminated (Lutwak *et al.* 2004).

3.18.2.2 Physics Package

3.18.2.2.1 Introduction

The physics package takes the instable 3.4-GHz signal from the LO and compares it with the internal frequency of the atoms. It generates an output signal that determines how much the LO frequency differs from the internal frequency of the atoms. In order to miniaturize a MEMS clock, various approaches have been investigated. Most of these, however, include the same general components and differ mostly in the engineered design. The first microfabricated physics package was reported in 2004 by the National Institute of Standards and Technology (NIST) (Knappe *et al.* 2004b). A picture is shown in Figure 8. It consisted of the VCSEL at the bottom, a micro-optical assembly, a vapor cell between two heaters, and a photodiode on the top. The electrical interconnects were wire bonds from the components in the stack to the pads on the baseplate.

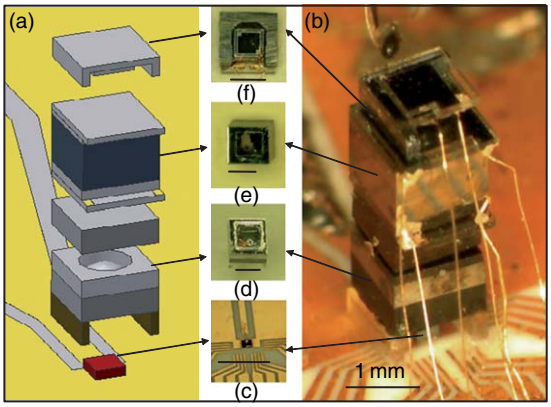

Figure 8 (a) Schematic and (b) photograph of a chip-scale atomic clock (CSAC) physics package consisting of (c) a vertical-cavity surface-emitting lasers (VCSEL), (d) an optics package, (e) a vapor cell with heaters, and (f) a photodetector.

In this approach, all the components were planar and in principle can be fabricated as arrays on individual wafers. While currently the wafers are diced first and the components stacked afterward, the design potentially allows for assembling the wafers first prior to dicing them into many individual physics packages, as indicated in Figure 9. This enables simple exchange of components and will potentially reduce fabrication costs.

Other groups have taken more complex approaches, where the laser beam is not just passed in a straight line to the photodetector. Lutwak *et al.*

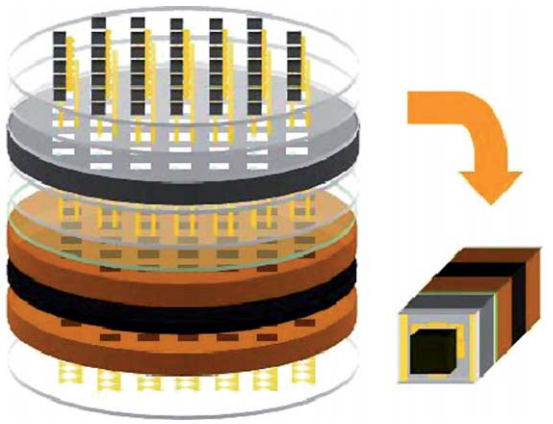

Figure 9 Wafer-level assembly of microelectromechanical systems (MEMS) clocks: wafers of baseplates with vertical-cavity surface-emitting lasers (VCSELs), spacers, neutral density (ND) filters with lenses, spacers, quarter waveplates, heaters, cells, and photodetectors are stacked and diced into individual chip-scale atomic clocks (CSACs) afterward.

(2004), for example, used a diverging beam and retro-reflected it back through the cell, where it was detected by a circular photodiode around the VCSEL die. One group explored a self-powered photon source as a low-power alternative to a VCSEL (Guo and Lal 2003). The kinetic energy of the electrons of 17.1 keV emitted from a radioactive ^{63}Ni film was used to generate photons through collisions with atoms. Photon generation in air, neon, and xenon was demonstrated with the goal to generate a low-power rubidium lamp for CSACs. Cesium, as well as rubidium, has been tried, and the fabrication of vapor cells differs. The cells vary in size between 250 µm and 1.5 mm. In the following sections as one example, we focus mainly on the approach taken by NIST, but there are other important ideas and approaches too.

3.18.2.2.2 Vertical-cavity surface-emitting laser

The VCSEL translates the electrical microwave signal from the LO into an optical beat signal. When the injection current of the VCSEL is modulated, a comb of modulation sidebands is created around the carrier in the optical spectrum spaced by the modulation frequency. The modulation properties of the VCSEL are therefore critical (see, e.g., Larsson *et al.* 2004). In order to interact with the atoms, the wavelength of the VCSEL has to be tuned such that some sidebands are resonant with optical atomic transitions.

VCSELs have been developed for telecom applications with high modulation bandwidths of up to 10 GHz (King *et al.* 1998, Lear *et al.* 1996). In contrast to traditional edge-emitting laser diodes, the light is reflected vertically through the thin layer of the active region, instead of along it. This creates a very short laser cavity of only a few micrometers between two stacks of Bragg mirrors, and only one longitudinal mode can be resonant with the gain medium (Jung *et al.* 1997). Nevertheless, many transverse modes could be resonating simultaneously (Chang-Hasnain *et al.* 1991, Degen *et al.* 2001). In oxide-confined VCSELs the physical restriction through a small aperture of about 3 µm diameter can limit oscillations to a single transverse TEM_{00} mode (Grabherr *et al.* 1997), reducing the output power of these single-mode devices to 5 mW (Jung *et al.* 1997, Seurin *et al.* 2002). Due to their vertical design, the beam profile is circular with a divergence angle of around 15°–25°. At the same time this design can allow two orthogonal polarization modes to be resonant. They can differ in frequency by many gigahertz and the polarization can flip back and forth between the two modes. Several approaches have been proposed to address this problem (Chavez-Pirson *et al.* 1993, Choquette and Leibenguth 1994, Debernardi and Gian Paolo 2003, Mukaihara *et al.* 1993, 1995a, Numai *et al.* 1995, Ostermann *et al.* 2005, Shimuzi *et al.* 1991). Nevertheless, these polarization jumps can still occur in single-mode VCSELs, and mode competition can cause amplitude noise in the single polarizations as well as in the total light power (Kaiser *et al.* 2002, Mukaihara *et al.* 1995b).

The vertical design makes it possible to fabricate large arrays of VCSELs, thus reducing the production costs (**Figure 10**). Their short cavities require Bragg mirrors of high reflectivity ($R > 99$ %), which reduce the sensitivity to optical feedback. Very low threshold currents below 1 mA (Choquette *et al.* 1994, Huffaker *et al.* 1994, Yang *et al.* 1995) have been reported, allowing small power consumption. At the same time, VCSELs have a large tuning of their output frequency with temperature ($\sim$30 GHz K^{-1}) and injection current ($\sim$300 GHz mA), which causes some problems for clock applications and places constraints on the current source and servo loops.

Even though laser linewidths of 3 MHz have been reported (di Sopra *et al.* 1999), most commercially available VCSELs have linewidths of around 50 MHz (Schmidt *et al.* 1996). While this can be a problem for many laser spectroscopy applications (Affolderbach *et al.* 2000), it does not substantially affect the CPT resonances. As mentioned in Section 3.18.1.3, the linewidth of the CPT resonance depends

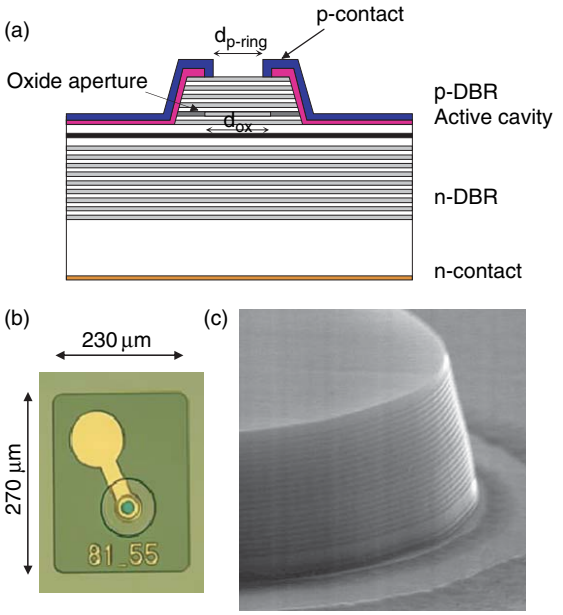

Figure 10 (a) Schematics and (b) photograph of a vertical-cavity surface-emitting laser (VCSEL). (c) Scanning electron microscope (SEM) picture of a VCSEL mesa after etching (before deposition of dielectrics and metal), the mesa height is about 3 µm. (Source: Avalon Photonics, Avalon Photonics Datacom VCSELs, http://www.avap.ch; reproduced with permission from Avalon Photonics Ltd.)

on the relative phase stability between the light fields, that is, the microwave phase, and not on the stability of the individual light fields (Dalton and Knight 1982). Nevertheless, a large VCSEL linewidth can reduce the CPT clock performance because of the large FM noise (Kitching *et al.* 2001c). The FM to amplitude modulation (AM) conversion process (Camparo 1998a) that occurs in the atoms adversely affects the CPT signal.

VCSELs have been developed for telecom applications since the 1980s (Fumio *et al.* 1989, Jewell *et al.* 1989), and reliable single-mode VCSELs have become available at the D_2 lines of Cs (852 nm). Lifetimes beyond one million hours have been reported (Avalon Photonics, Honeywell, Ulm Photonics, Mukoyama *et al.* 2006). Recently, VCSELs at the D_1 lines of Cs (895 nm) and Rb (795 nm), and D_2 lines of Rb (780 nm) and potassium (766 nm) have been produced.

Since their structure consists of more than 100 layers and their fabrication processes and designs vary from one manufacturer to another, the characteristics of single-mode VCSELs vary and directly impact the clock performance (see, e.g., Kwakernaak *et al.* 2004). It is therefore critical to choose the right VCSEL for the specific CSAC design. In order to get high yields, MEMS clocks must conform to stringent requirements regarding epitaxial growth accuracy and uniformity, which is much more demanding than is typically achieved in the best semiconductor fabrication facilities (Serkland *et al.* 2006). Some of the specifications are summarized here:

- Tunable to precise atomic wavelength (preferably 795 or 894 nm) at a given operating temperature, e.g., 75°C, ±5°C (Serkland *et al.* 2006).
- Single longitudinal, transverse, and polarization mode.
- Phase modulation index, >1.8 reachable with radio frequency (RF) powers of −6 dBm at 3.4 GHz (Brannon *et al.* 2005) or 0 dBm at 4.6 GHz (Serkland *et al.* 2006).
- Linewidth, <100 MHz (Serkland *et al.* 2006).
- Power consumption, <3 mW.
- Optical output power, 50 µW–1 mW.

3.18.2.2.3 Vapor cells

The vapor cell can be viewed as the heart of the clock, as it contains the atoms. Besides being a container that does not react with the atoms, the cell has to provide access to the light to and from the atoms. It needs to withstand elevated temperatures, should not be magnetic, and has to be hermetically sealed. For chip-scale vapor cells it should furthermore allow for wafer-level fabrication and filling, since fabrication cost as well as uniformity over an ensemble of cells is of concern. The interior size of the cell should be in millimeters and the exterior volume should be as small as possible. Finally, the geometry of the cell needs to be considered, when integrated with the rest of the physics package.

Several millimeter-sized glass vapor cells have been reported using conventional glass-blowing techniques (Balabas *et al.* 2006) or a focused CO_2 laser (Knappe *et al.* 2003a) (**Figure 11**). Glass alkali cells have been well studied for use in optically pumped clocks. This can make the wall effects due to higher surface-to-volume ratio and thinner walls more predictable. However, the high surface tension of glass, as well as the possibility of the alkali atoms reacting with the glass at high temperatures, makes size reduction to 1 mm challenging.

In an attempt to fulfill the above requirements for a miniature alkali vapor cell, a first fabrication process based on MEMS silicon wafers etching techniques was proposed (Kitching *et al.* 2002). At present, most fabrication techniques for microfabricated cells rely on these ideas, while the actual techniques for filling the

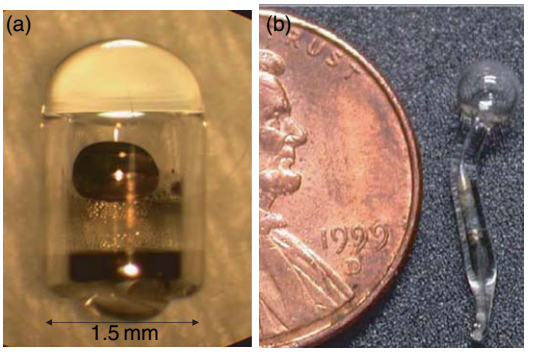

Figure 11 Photographs of small vapor cells: (a) made from a hollow-core glass fiber with a CO_2 laser; (b) made with conventional glass-blowing techniques.

cells with alkali atoms differ significantly. The first MEMS-fabricated vapor cells (Knappe *et al.* 2003b, Liew *et al.* 2004) used double-side polished ⟨100⟩ silicon wafers that were photolithographically patterned inside a clean room (**Figure 12**) and subsequently etched by means of silicon etching techniques (potassium hydroxide (KOH) or deep reactive ion etching (DRIE)) to produce arrays of holes. This allows for a very high level of miniaturization as well as regular arrays of cells with tight tolerances. Cells with holes of 1 mm in size were also successfully made by diamond drilling (Liew *et al.* 2004) or ultrasonic drilling. While surface roughness of the interior walls could be of concern for cells with antirelaxation wall coatings (Alexandrov *et al.* 2002, Bouchiat and Brossel 1966, Robinson *et al.* 1958), no evidence of effects due to rough silicon walls have been published so far for buffer gas cells.

Two early approaches for filling and sealing microcavities with alkali atoms have been demonstrated by NIST (Liew *et al.* 2004). Both used anodic bonding (Wallis and Pomerantz 1969) of Corning 7740 glass (Pyrex™)[1] or borosilicate glass to the etched silicon chips to create a cell preform. The cell was then sealed under a buffer gas atmosphere by anodically bonding a second piece of Pyrex over the top of the preform. In the first method, cesium was injected into the preform with a micropipette in an anaerobic chamber (**Figure 13**). While this is a very simple and inexpensive way to make cells, the chamber environment was difficult to control precisely. First, residual oxygen in the chamber limited the lifetime of cesium and produced large amounts of oxidized cesium inside the cell. Second, other background gases were present inside the chamber and thus inside the cell, which can cause

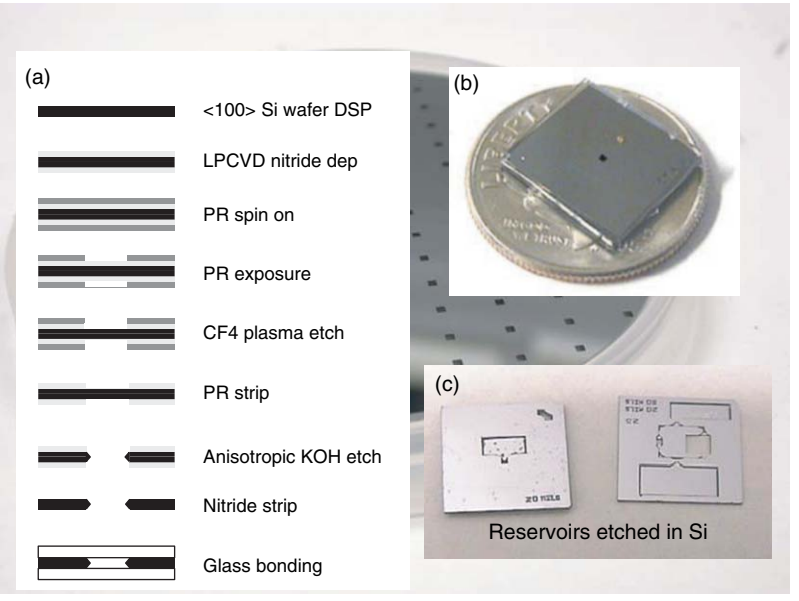

Figure 12 Microelectromechanical systems (MEMS) etching process of microfabricated vapor cells. (a) Steps of a typical potassium hydroxide (KOH) etching process. (b) Photograph of a wafer chip with etched hole and glass bonded onto both sides of the chip. (c) Photograph of chips with channels and reservoirs etched into them in addition to a hole. *Background*: Photograph of a 4″ wafer with an array of holes.

[1]Trade name is stated for technical clarity and does not imply endorsement by NIST. Products from other manufacturers may perform as well or better.

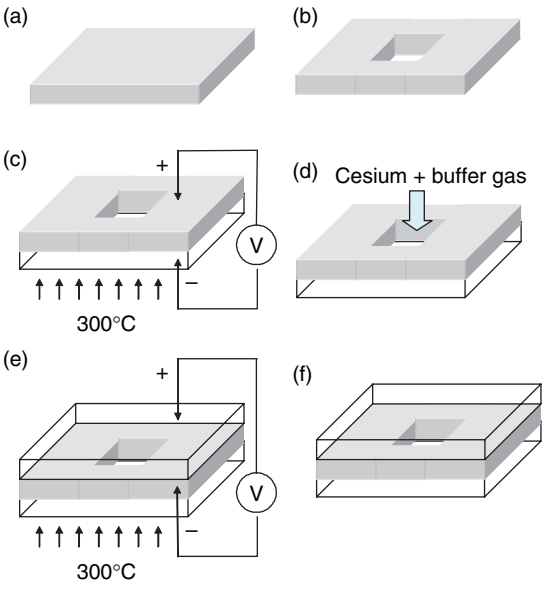

Figure 13 Schematic of cell fabrication based on silicon etching and anodic bonding. A Si wafer (a) with holes etched through it (b) is anodically bonded to a piece of glass (c). It is then filled with alkali atoms and buffer gas (d), and a second piece of glass is bonded on top (e) to form a robust, hermetically sealed vapor cell (f).

problems when trying to reduce the temperature coefficient of the clock by using controlled mixtures of different buffer gases (Vanier *et al.* 1982) (see Section 3.18.4.3 for a more detailed discussion). Very similar filling techniques have been reported subsequently by Kwakernaak *et al.* (2004) and Lutwak *et al.* (2005).

The second filling technique was successfully used in centimeter-sized buffer gas vapor cells before. A stable cesium compound was deposited into the cell and was reacted to produce pure cesium metal by using the following process (Espe 1966):

$$BaN_6 + CsCl \rightarrow BaCl + 3N_2 + Cs$$

The decomposition was initiated by heating the mixture to roughly 200°C inside a UHV chamber. The problem in a small cell arose from the difficulty of pumping off the excess nitrogen gas formed without having all the cesium metal leave the small cell volume at elevated temperatures. Furthermore, the BaCl and the free barium remained inside the cell where the chemical solution was deposited. In bigger cells, this can be desirable because barium can be used as a getter. However, in small cells that are heated to higher temperatures, the gettering rate of nitrogen by barium can cause pressure changes in the cells that result in frequency changes (Knappe *et al.* 2005a). Since the clock frequency of cesium is extremely sensitive to the nitrogen pressure ($45 \pm 2\,\mathrm{Hz\,kPa^{-1}}$; Beverini *et al.* 1981), the pressure has to be stable at 2×10^{-3} kPa to support a frequency stability of 1×10^{-11}. When using barium inside small buffer gas cells, nitrogen must be completely avoided and instead atoms such as inert gases can be used. But even then it can be difficult to ensure that the chemical reaction has been completed and that no nitrogen is left inside the cell.

One advantage of chloride reduction through barium is that it is relatively easy and cheap to produce small quantities of isotopically enriched ^{87}Rb. Usually, isotopical purity of ^{87}Rb is preferred so that the light is not absorbed by the ^{85}Rb atoms (with 62% natural relative abundance), for which the CPT condition is not fulfilled. In order not to have any residues inside the cell cavity, the alkali atoms can be produced this way inside a glass ampoule and evaporated into the cell cavity through a small nozzle (Knappe *et al.* 2005a). The cell is then closed after filling the chamber with the desired buffer gas mixture. This is a versatile technique, and the cells with Cs, ^{87}Rb, and ^{85}Rb and a variety of buffer gases with pressures <1 torr to 1 atm have been produced this way.

Other approaches to insert the alkali atoms into MEMS cell cavities have also been reported on since then. Radhakrishnan and Lal (2005) encapsulated rubidium in wax micropackets as shown in **Figure 14**. The cell preforms were made by anodic bonding of bulk-micromachined silicon wafers to Pyrex under a xenon atmosphere. One side of the cavity array has a silicon

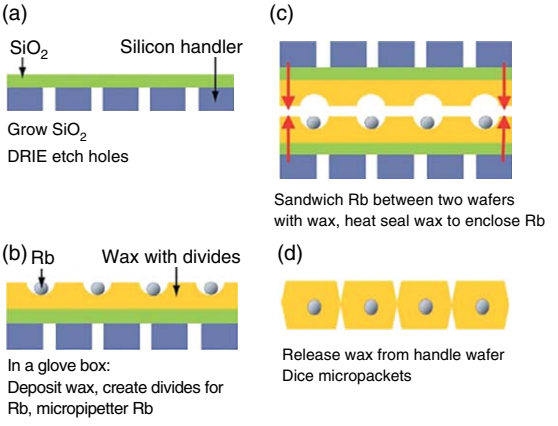

Figure 14 Process to enclose Rb in wax micropackets. (Source: Radhakrishnan S, Lal A 2005 Alkali metal-wax micropackets for chip-scale atomic clocks. *Dig. Tech. Papers – Int. Conf. Solid State Sensors and Actuators and Microsystems, Transducers '05*, pp. 23–6, © 2005; reproduced with permission from IEEE.)

nitride membrane that gets thermally bonded to the wax micropackets, as shown in **Figure 15**. The rubidium is released into the cavity by laser ablation of the silicon nitride membrane. Rubidium absorption was measured in these cells successfully, but the effect of the wax on the ground-state hyperfine coherence has not been studied yet.

A wafer-level process to make arrays of nitrogen buffer gas cells with cesium has been developed by Liew *et al.* (2006a, b). Here, cesium azide (CsN_3) is evaporated through an aluminum shadow mask into cell preforms made from silicon with borosilicate glass windows. The cavities are closed under vacuum by anodically bonding a wafer of borosilicate glass onto the top. The cesium azide is decomposed into cesium and nitrogen by exposing the cells to ultraviolet light. The decomposition is stopped when the nitrogen pressure reaches the desired value.

A technique demonstrated by Gong *et al.* (2006) uses cesium-enriched glass as a source for alkali atoms in microfabricated cells. The glass pieces are melted into a well on the bottom of an anodically bonded cell preform (**Figure 16**). The cell is closed by anodic bonding under the desired buffer gas atmosphere. Finally, the cesium atoms are released from the glass by passing an electrolytic current through the glass at 500°C and 1 kV between a $NaNO_3$ anode and the silicon (cathode).

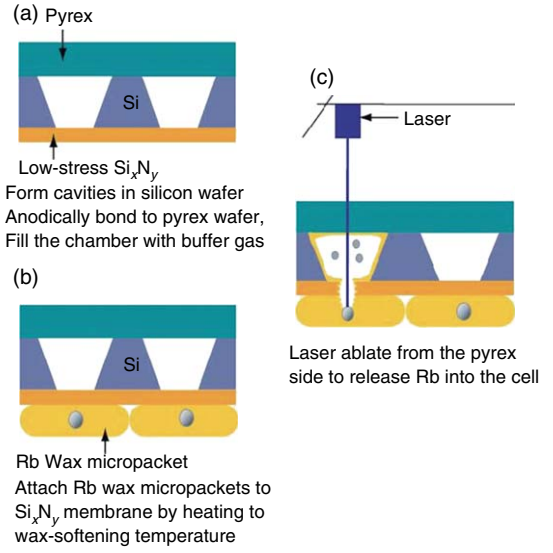

Figure 15 Process outline to realize Rb vapor cells using Rb wax micropackets. (Source: Radhakrishnan S, Lal A 2005 Alkali metal-wax micropackets for chip-scale atomic clocks. *Dig. Tech. Papers – Int. Conf. Solid State Sensors and Actuators and Microsystems, Transducers '05*, pp. 23–6, © 2005; reproduced with permission from IEEE.)

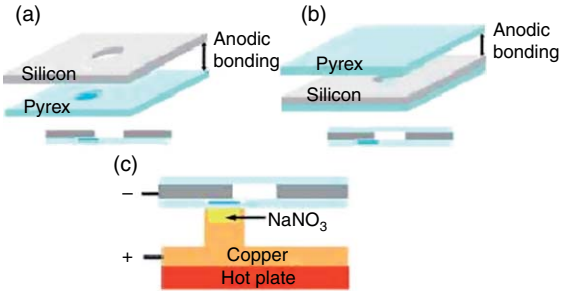

Figure 16 Schematic of the electrolytic cell filling process. (a) A Si wafer with a hole of 2.5 mm diameter is anodically bonded to a Pyrex wafer with a shallow well, 2.5 mm in diameter. Pieces of Cs-enriched glass (dark blue) are melted into the well. (b) Another Pyrex wafer is anodically bonded to the other free surface of the silicon wafer under an argon cover gas. (c) A copper stem, containing molten $NaNO_3$ salt in a basin at the top, is pressed against the Pyrex below the Cs glass well. The stem is attached to the copper base, resting on a hot plate at a temperature of 500°C. A potential of +700 V is applied for a few minutes between the molten $NaNO_3$ anode and the silicon cathode. (Source: Gong F, Jau Y Y, Jensen K, Happer W 2006 Electrolytic fabrication of atomic clock cells. *Rev. Sci. Instrum.* 77, 076101, © 2006; reproduced with permission from American Institute of Physics.)

A MEMS glass-blowing technique has been reported by Erklund and Shkel (2006). As the schematic in **Figure 17(a)** explains, cavities are etched into one side of a silicon wafer using DRIE. A 100-μm-thick piece of borosilicate glass is then anodically bonded over the top of the cavities enclosing the atmospheric pressure. When the wafer is heated to 850°C, that is, above the melting point of the glass, the air pressure inside the cavities deforms the glass into spherical shapes, as shown in **Figure 17(b)**. Afterward, the backside of the cavities is etched to allow for filling with alkali atoms. ^{87}Rb cells have been made this way by using the evaporative filling method described previously and by anodically bonding a second piece of borosilicate glass over the backside in the presence of a nitrogen and xenon atmosphere.

3.18.2.2.4 Optics

Even though the actual designs of the physics packages vary significantly, in almost all cases, there is an optics package that controls the size, intensity, and polarization of the laser beam. Most approaches use circular polarization by passing the beam through a low-order quarter waveplate. Neutral density (ND) filters are a simple way to attenuate the light to the desired power of around 10 μW. At the same time, these attenuators can reduce the optical feedback

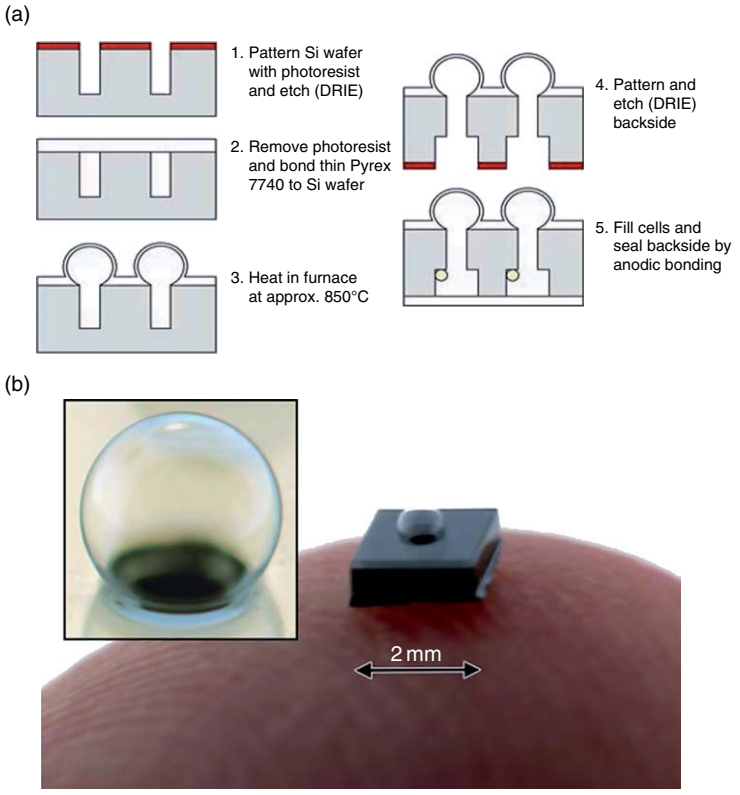

Figure 17 (a) Wafer-level fabrication of glass-blown vapor cells. (b) Photograph of a micro glass cell on top of a silicon wafer. (Courtesy of J. Erklund).

produced by light that gets reflected back into the VCSEL. Some optics packages also use antireflection-coated elements. In some setups, a polarizer is inserted to filter out the undesired polarization modes (Gerginov 2006). While in many designs the laser beam is collimated by a microlens, it has been shown that this is not necessary and a diverging beam can be used instead (Lutwak *et al.* 2004). **Figure 18** shows an example of an optics package consisting of a spacer, a ND filter, an inkjet-printed epoxy lens, and a quarter waveplate through which the beam passes. Other designs use more complicated beam paths by implementing micromirrors in the optics package.

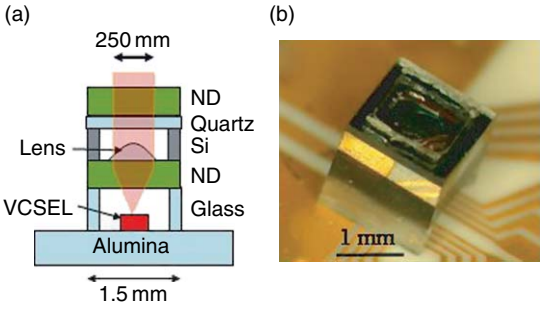

Figure 18 Schematic (a) and photo of a chip-scale atomic clock (CSAC) optics package.

3.18.2.2.5 Heating

In order to achieve sufficient absorption of the laser light over a 1 mm path length, the alkali vapor pressure has to be increased from its room temperature. Because most cells contain a liquid or a solid drop of alkali metal along with the vapor, this is usually done by simply heating the cell. The temperature for 50% absorption of the resonant light depends also on the buffer gas pressure, since buffer gas collisions change the lifetime of the P states (Allard and Kielkopf 1982). For higher pressures and low laser powers, the alkali density has to be increased proportional to the increase in buffer gas pressure to maintain the same absorption. For a 20-kPa nitrogen cell, for example, this temperature is around 75°C for cesium and 90°C for rubidium. Furthermore, it is advantageous to maintain the cell windows at a temperature slightly higher than the body of the cell to minimize the quantity of the alkali atoms that condense on the windows.

Microfabricated heaters are not a new technology (Lai *et al.* 1995, Nguyen and Howe 1993, Ruther *et al.* 2004) and approaches differ significantly. To reduce the magnetic fields produced by the currents flowing through the resistive heaters, patterned traces are often meandered and retraced and resistances are chosen such that only small currents flow. Traces can also be made from transparent materials or patterned such that the laser beam can pass through the center of the cell for better uniformity of heat distribution (Lutwak *et al.* 2004). Furthermore, thin substrate materials with low thermal conductivities are used for better thermal insulation. Substrates, heaters, and temperature sensor materials are chosen to be least magnetic, e.g., platinum, glass, polyimide, indium tin oxide (ITO).

Figure 19 shows an example of microfabricated transparent heaters (Schwindt *et al.* 2006) made from ITO. The heaters are glued directly onto the cell windows, and heat is produced when current flows through the conductive ITO layers. Two glass substrates with patterned ITO are glued together with a nonconductive epoxy to reduce the magnetic fields. The lighter color lines in the heater are where ITO has been removed through laser patterning. After the ITO patterning, gold pads are deposited for wire bonding, and a 2-μm insulating layer of benzocyclobutene is deposited over the remaining exposed ITO so that the electrical contact between the upper and the lower ITO layers is made only through the gold pads. The large arrows show where current enters and exits the heater. The electrically conductive epoxy provides the connection between the upper and the lower ITO. **Figure 20** shows a vapor cell with integrated heaters made from boron-doped silicon. The doped bifilar traces are bulk-micromachined into the silicon cell preform with a high aspect ratio (Liew *et al.* 2005, 2006b).

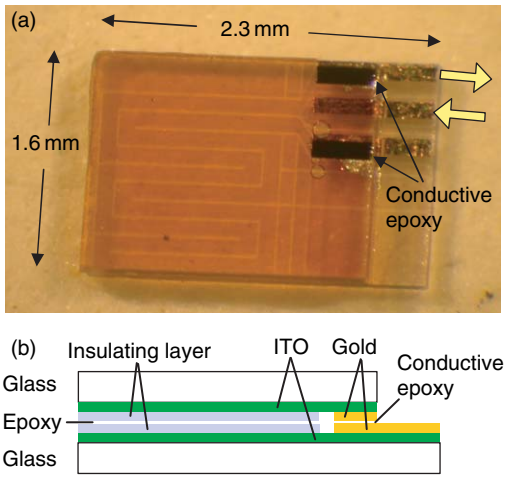

Figure 19 (a) Photograph and (b) schematic side view of laser-patterned indium tin oxide (ITO) heater. (Source: Schwindt P D D, Lindseth B, Knappe S, Shah V, Kitching J 2006 A chip-scale atomic magnetometer with improved sensitivity using the Mx technique. *Appl. Phys. Lett.*)

3.18.2.2.6 Magnetic field control

Most CSACs are operated on the $m_F = 0 \leftrightarrow m_F = 0$ hyperfine transition, to be insensitive to magnetic fields in first order. The magnetic field shifts the neighboring Zeeman sublevels apart with $\sim 7\,\text{kHz}\,\mu\text{T}^{-1}$ for ^{78}Rb and $\sim 3.5\,\text{kHz}\,\mu\text{T}^{-1}$ for Cs. Therefore, a field of a few microtesla in strength is sufficient to separate the neighboring CPT resonances of a few kilohertz linewidth. In order to couple the two 0–0 hyperfine components with circularly polarized light, a longitudinal magnetic field is required.

Until now, not much has been published about how to precisely control the magnetic field in the vicinity of the tiny vapor cell. Nevertheless, magnetic field strength, homogeneity, and direction can be of concern. The amplitude of the CPT 0–0 resonance is proportional to $\cos^2(\theta)$, where θ is the angle between the

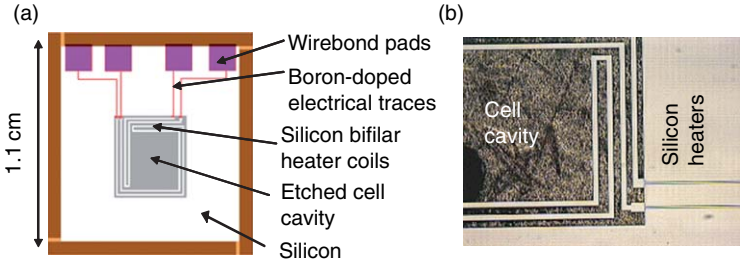

Figure 20 (a) Design of an advanced cell with integrated heaters. (b) Photograph of closeup of the cell cavity. (Source: Liew L, Moreland J, Knappe S, Shah V, Schwindt P, Gerginov V, Kitching J, Hollberg L 2005 Microfabricated alkali atom vapor cells with in-situ heating for atomic-based sensors. *Proc. 3rd Int. Symp. Sensor Science*, Juelich, Germany, pp. 181–3.)

direction of laser propagation and the magnetic field (Wynands and Nagel 1999). Also, because fairly high buffer gas pressures are used in most cells, the atoms can be considered stationary and sample the magnetic field at their location. The CPT resonance is then a convolution of all atoms interrogated and therefore broadens with magnetic field gradients across the cell. But again, if the 0–0 transition is used in buffer gas cells, this effect is reduced because the 0–0 resonance shifts with the magnetic field in second order only. It could be further reduced by using antirelaxation wall-coated cells (Robinson *et al.* 1958), where motional narrowing (Bloembergen *et al.* 1948, Kleppner *et al.* 1962) would suppress the gradient-induced broadening. Finally, the CPT 0–0 resonance frequency shifts with the total magnetic field at $57.5\,\mathrm{mHz}\,\mu\mathrm{T}^{-2}$ for cesium and $42.7\,\mathrm{mHz}\,\mu\mathrm{T}^{-2}$ for ^{87}Rb (see, e.g., Steck 1998, 2001, and references therein).

The externally applied offset field should therefore be made as small as possible to reduce frequency shifts and broadening due to ambient field changes (e.g., through heater currents), but big enough to lift the Zeeman degeneracy beyond the CPT linewidth and to ensure that ambient fields are not rotating the direction of the total field too much (e.g., earth's magnetic field). The external offset field is applied through either magnetic coils or permanent magnets. The latter method has the advantage of reducing the power consumption of the CSAC and the residual magnetic fields because the heater supply leads are not present. The disadvantage is that the CSAC frequency cannot be tuned through the C-field (as is most commonly used in Rb vapor clocks). The physics package is usually shielded from external magnetic fields, for example, the earth's magnetic field, by at least one layer of material with high permeability. It has been shown that shielding factors of around 1000 for one layer and greater than 4×10^6 (Hodby 2006) for three-layer shields of several millimeters in size can be reached.

3.18.2.3 Local Oscillator

3.18.2.3.1 Introduction

Most of the CSACs described so far are passive atomic clocks (see Section 3.18.2.1). The clock frequency is produced by a LO, which is locked to the atomic CPT resonance with a loop bandwidth $\mathrm{BW_{lock}}$. The clock frequency is determined by the atomic ground-state hyperfine frequency, i.e., 6.834 GHz for ^{87}Rb or 9.192 GHz for ^{133}Cs. Using CPT interrogation, a modulation of the VCSEL at half these frequencies is possible. Many applications, however, require a clock with an output frequency of 10 MHz, and frequencies up to 100 MHz can probably be used. Therefore, either the LO frequency has to be divided for the output or a low-frequency LO (10 MHz, for example) should be multiplied for VCSEL modulation. For reaching the goal of 30 mW total power consumption for the CSAC, the output frequency should most likely be the specific gigahertz frequency, determined by the atoms. In the following, we will mostly focus on LOs at microwave frequencies, which are developed for the chip-scale clocks. The list presented here is not complete but is rather a condensed overview.

As a passive standard, the CSAC frequency stability at times shorter than $(\mathrm{BW_{lock}})^{-1}$ is determined mostly by the phase noise of the LO. To reach a clock frequency stability of 1×10^{-11} at 1 h of integration, the single-sideband phase noise power spectral density of the LO needs to be between $-25\,\mathrm{dBc\,Hz^{-1}}$ at 100 Hz offset (Brannon *et al.* 2005, Kitching 2003) and $-43\,\mathrm{dBc\,Hz^{-1}}$ at 300 Hz offset (Römisch and Lutwak 2006) from the carrier. The required output power depends largely on the modulation efficiency of and the coupling efficiency to the VCSEL. It has been shown that for some VCSELs <-6 dBm output power at 3.4 GHz can be sufficient to transfer 60% of the light power into the desired first-order sidebands (Brannon *et al.* 2006b). At 4.6 GHz, the requirement was set to 0 dBm (Römisch and Lutwak 2006). In order to reach the goal of total power of 30 mW for the CSAC, it would be desirable if the DC power consumption of the LO was well below 10 mW and the footprint below 1 $\mathrm{cm^2}$.

A significant concern is the thermal frequency drift of the voltage-controlled oscillator (VCO). Since it is most likely not actively temperature-stabilized, its resonance frequency must not drift out of the tuning range provided by the servo when the ambient temperature varies over the entire operating range of the clock. A maximal thermal frequency shift of around $\pm 10\,\mathrm{ppm\,K^{-1}}$ was therefore a goal with a tuning range of a few megahertz. At the same time, the tuning range of the VCO should be small for good resolution and frequency stability, but should be large enough to compensate for manufacturing tolerances. Finally, a supply voltage below 3.5 V is desired and all the components should be of low cost.

The best available oscillators at gigahertz frequencies are dielectric resonator oscillators (DROs) with Q factors of several thousand (Pozar 2001) and even 100 000 for cryogenically cooled sapphire devices (Ivanov and Tobar 2006, Ivanov *et al.* 1998). But their size, weight, and power make them unsuitable

for MEMS clocks. Crystal oscillators can be very good with similar *Q*s in the frequency range of up to hundreds of megahertz (Vig 1992). Oven-controlled devices (OCXOs) have very good stability, but require several hundred milliwatts of power, but TCXOs or microprocessor-controlled (MCXO) crystal oscillators can operate on a few milliwatts. Nevertheless, multiplying their frequencies into the gigahertz region may require too much power for CSACs. Therefore, considerable research is done on alternative approaches of small, low-power LOs at gigahertz frequencies.

3.18.2.3.2 Oscillator designs for CSAC

Even though the development of VCOs for MEMS clocks has advanced rapidly, not many devices have currently been tested together with CSAC physics packages. One reason is the requirement to operate exactly at the resonance frequency of the atoms.

Popović and coworkers implemented two oscillators at 4.596 GHz and 3.417 MHz (Brannon *et al.* 2005, 2006a) and demonstrated their applicability to a CSAC. The oscillators were based on quarter-wavelength ceramic-filled coaxial resonators. The phase noises of the oscillators were measured to be better than $-35\,\mathrm{dBc\,Hz^{-1}}$ at 100 Hz and $-94\,\mathrm{dBc\,Hz^{-1}}$ at 10 kHz. A weakly coupled varactor diode provides a tuning range of ~3 MHz to compensate for a temperature instability between 0 and $40\,\mathrm{ppm\,K^{-1}}$ over −5°C to +65°C. DC powers of 2.1 and 13.9 mW resulted in −6 dBm output power at 3.4 GHz and −4 dBm at 4.6 GHz. All components were of low cost and were commercially available.

A 3.417-MHz VCO was integrated with a CSAC ^{87}Rb physics package (Brannon *et al.* 2006b) onto a common baseplate. A power of −6 dBm was sufficient to modulate the VCSEL at its desired modulation depth. **Figure 21** is a photograph of the low-power 3.4-GHz oscillator (Brannon *et al.* 2006b) and the CSAC physics package.

Römisch and Lutwak (2006) recently demonstrated a 4.596-GHz oscillator based on a thin-film temperature-compensated resonator (Römisch and Lutwak 2006) using a very similar oscillator design. A single-sideband phase noise power spectral density of $-38\,\mathrm{dBc\,Hz^{-1}}$ at 300 Hz was measured when emitting the required 0 dBm output power, improving at lower powers. With a power consumption below 10 mW and a tunability of $2\,\mathrm{MHz\,V^{-1}}$, this resonator was designed for cesium CSAC.

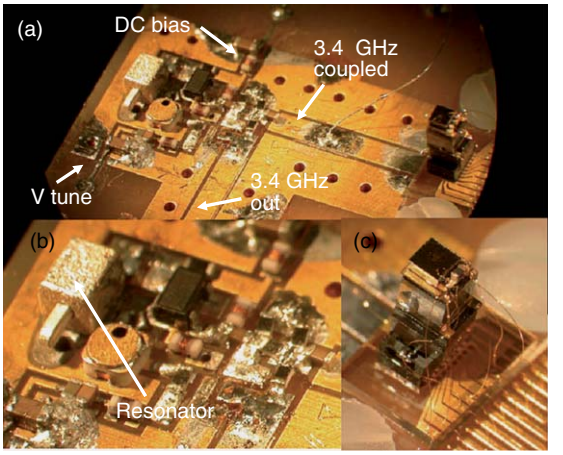

Figure 21 (a) Photograph of a 3.4-GHz voltage-controlled oscillator (VCO) integrated with a chip-scale atomic clock (CSAC) physics package. Inputs are DC bias and tune voltage for the VCO, and laser bias, photodetector bias, and heater currents for the physics package. Outputs are stabilized at 3.4 GHz and diagnostic signals. (b) Closeup view of the VCO and (c) the physics package.

3.18.2.3.3 Other MEMS resonators

The oscillators described so far were able to reach the goals set for the CSAC in terms of frequency stability, power consumption, and size. Nevertheless, fully integrated MEMS oscillators can be advantageous for mass fabrication and possibly advanced performance. A detailed noise analysis of MEMS oscillators was performed (Vig and Yoonkee 1999). In the following, we introduce a few approaches using other types of MEMS resonators.

Totally integrated complementary metal oxide semiconductor (CMOS)-type oscillators are probably the smallest devices, but do not presently fulfill the phase noise requirements (Gierkink *et al.* 2003, Mourant *et al.* 2000). Much progress has been made recently in the development of micromachined mechanical resonators (Nguyen 2005). Unloaded *Q*s greater than 10 000 have been demonstrated up to 1.5 GHz (Li *et al.* 2004) and temperature stabilities below 1.8×10^{-5} over 25–125°C (Hsu and Nguyen 2002). An advantage of these micromechanical resonators based on polysilicon (Li *et al.* 2004) or diamond (Wang *et al.* 2002) surface micromachining is that their resonance frequency can be defined by their lateral dimension, rather than by their thickness, which allows for easy specification through computer-aided design (CAD). Furthermore, arrays of mechanically coupled 15-MHz resonators have demonstrated an improvement in phase noise of 40 dB by locking all resonator frequencies to one

mode (Lee and Nguyen 2004). Nevertheless, no oscillator using one of these micromachined resonator tank has been demonstrated in the gigahertz region as at the time of this writing (2006).

MEMS techniques lend themselves to the making of gigahertz oscillators for CSACs, as small size allows for faster speed, lower power consumption, and lower cost. In the case of quartz resonators, MEMS fabrication enabled quartz on-chip resonators at 900 MHz with *Q*s greater than 10 000 and strong third overtone modes above 2.5 GHz and *Q*s greater than 7500 (Kubena *et al.* 2005, Stratton *et al.* 2004). Temperature coefficients around $-5\,\text{ppm}\,\text{K}^{-1}$ have been measured in shear strip designs. The fabrication process and a scanning electron microscope (SEM) photograph of a complete ultrahigh frequency (UHF) quartz resonator are shown in **Figure 22** as an example.

Other interesting candidates include thin-film bulk acoustic resonators (FBAR) and high-tone bulk acoustic resonators (HBAR). Frequency-tunable FBAR oscillators at 2 GHz showed a phase noise of $-112\,\text{dBc}\,\text{Hz}^{-1}$ at 10 kHz and an unloaded *Q* better than 500 (Khanna *et al.* 2003). With a supply voltage of 3.3 V, it uses 115 mW of power and had a tuning

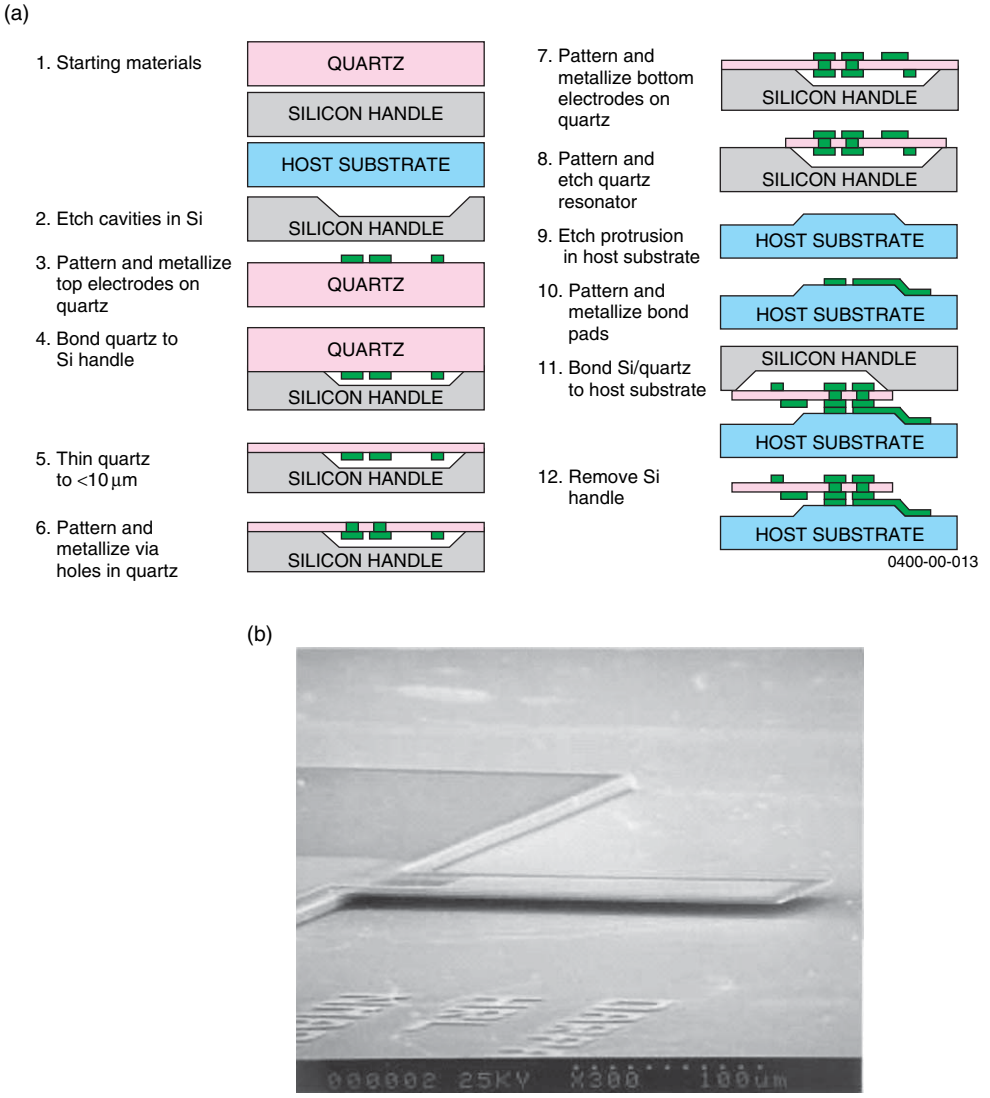

Figure 22 (a) Fabric flow for a microelectromechanical systems (MEMS)-based quartz resonator. (b) Scanning electron microscope (SEM) photograph of a completed ultrahigh frequency (UHF) resonator with 2-mm quartz thickness. (Source: Kubena R L, Stratton F P, Chang D T, Joyce R J, Hsu T Y, Lim M K, M'closkey R T 2005 MEMS-based quartz oscillators and filters for on-chip integration. *Proceedings of the 2005 IEEE International Frequency Control Symposium and Exposition*, pp. 122–27, © 2005; reproduced with permission from IEEE.)

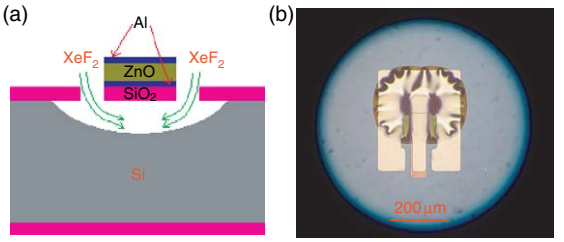

Figure 23 (a) Cross-section schematic of an Al/ZnO/Al/SiO_2 film bulk acoustic resonator (FBAR) and (b) photograph of the fabricated FBAR. (Source: Zhang H, Kim J, Pang W, Yu H, Kim E S 2005 5 GHz low-phase-noise oscillator based on FBAR with low TCF. *The 13th Int. Conf. Solid-State Sensors, Actuators and Microsystems, Dig. Tech. Papers (Transducers '05)*, pp. 1100–1, © 2005; reproduced with permission from IEEE.)

sensitivity of 180–370 kHz V^{-1} (0–10 V tuning range). FBAR resonators generally have temperature stabilities of 20–30 ppm K^{-1}. Pang *et al.* (2005) have reduced the temperature coefficient of a tunable FBAR resonator at 2.8 GHz by 40 ppm K^{-1} by integrating a micromachined air-gap capacitor and Zhang *et al.* (2005) demonstrated a temperature stability of −8.7 ppm K^{-1} with a 5-GHz CMOS-compatible device. Care has to be taken in the design of FBAR oscillators to satisfy the resonance condition for the desired mode only, as they can have closely spaced series and parallel resonances. A schematic and a photograph of a 5-GHz FBAR oscillator are shown in **Figure 23**.

Resonators can be scaled even smaller with nanoelectromechanical systems (NEMS) to allow for Q factors in the range of 1000–100 000 with very low power consumption. Double-clamped beams made from SiC reach microwave frequencies (Ekinci and Roukes 2005).

3.18.2.4 Control Electronics

Besides the physics package and the LO, the CSAC needs miniaturized control electronics for operating the clock by providing the supply currents and voltages for the individual components and for controlling at least four servo loops for laser and cell temperature, laser frequency, and LO frequency. Sometimes, laser and cell are maintained at the same temperature and the two servos can be combined.

To reach the goal of 1 cm^3 total volume for the CSAC, an application-specific integrated circuit (ASIC) will most likely be required. Until now, prototypes of 10 cm^3 have been demonstrated (Gerginov *et al.* 2005, Lutwak *et al.* 2005) with control electronics

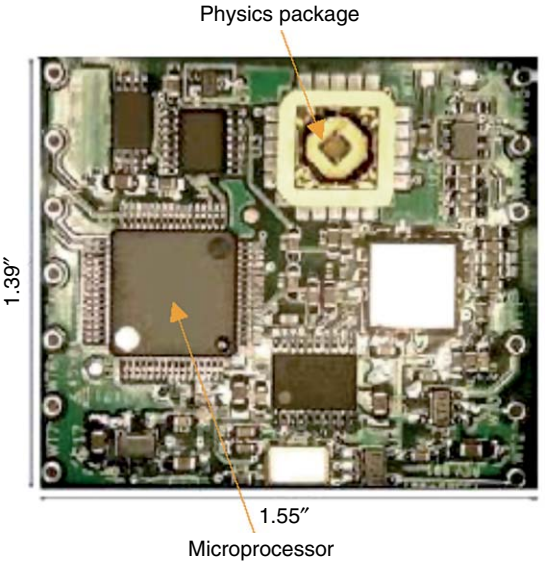

Figure 24 Prototype printed circuit (PC) board for a miniature atomic clock. (Source: Lutwak R, Vlitas P, Varghese M, Mescher M, Serkland D K, Peake G M 2005 The MAC – A miniature atomic clock. *Joint Meeting of the IEEE International Frequency Control Symposium and the Precise Time and Time Interval (PTTI) Systems and Applications Meeting*, Vancouver, BC, Canada, pp. 752–7.)

based on digital microprocessors. **Figure 24**, for example, shows a printed circuit (PC) board of footprint 14 cm^2 containing all the control electronics necessary to run a CSAC. As shown in the block diagram in **Figure 25**, the analog signals from the CSAC are converted into digital signals and processed by the microprocessor. The output is converted into analog signals again, which in turn drive the CSAC.

The temperatures are usually measured by thermistor temperature sensors. A proportional integrator (PI) servo is programmed into the microprocessor chip and the single-sided (heating only) output controls the heater currents. For low power consumption, the cell and the laser are operated above the maximum ambient temperatures, so that no cooling is required.

Since the laser and the LO have to be locked to the center of the optical and microwave resonance lines, respectively, phase-sensitive detection is implemented for these two servos. The laser current and the LO tuning voltage are modulated at a low frequency (500 Hz–30 kHz), and the photodetector voltage is demodulated at this frequency. To prevent cross-talk between the two loops, the two modulation frequencies are usually chosen to be different by an order of magnitude and the demodulation filters have to be tuned accordingly. The phase of the

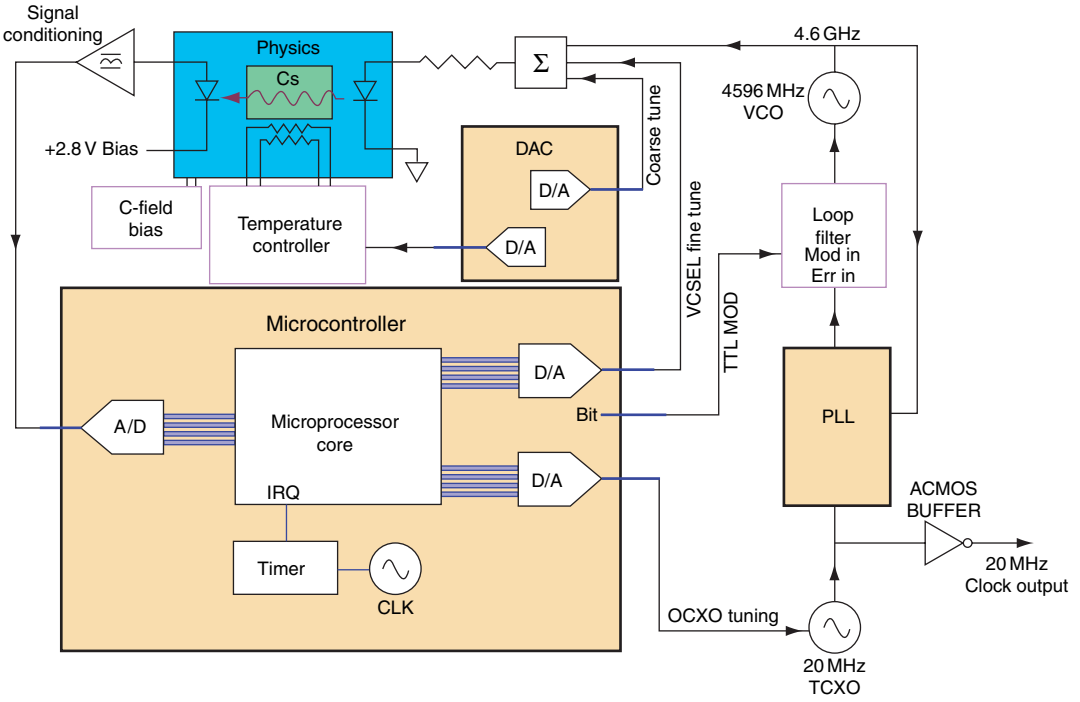

Figure 25 Block diagram of a miniature atomic clock. (Source: Lutwak R, Vlitas P, Varghese M, Mescher M, Serkland D K, Peake G M 2005 The MAC – A miniature atomic clock. *Joint Meeting of the IEEE International Frequency Control Symposium and the Precise Time and Time Interval (PTTI) Systems and Applications Meeting*, Vancouver, BC, Canada, pp. 752–7.)

demodulation has to be chosen precisely for best performance. Due to the high tunability of VCO ($\sim$2 MHz V^{-1}) and VCSEL ($\sim$300 GHz mA^{-1}), highly stable supply voltage and current are needed. In order to run the CSAC off a common voltage supply, for example, two AA batteries (3 V), heater resistances and current supplies have to be designed for minimum power consumption at this voltage.

3.18.2.5 Packaging

When power consumption is the concern, packaging, especially for the physics package, becomes a critical issue. Since laser and cell are heated above the ambient temperature, that is, to at least 75°C for many applications, thermal management and control need to be addressed. Without this control, physics packages will require 100–250 mW just to heat the small vapor cell and tiny laser die (Kitching *et al.* 2004). Most of the heating power is then lost thermally through conduction and convection.

Conduction can be tremendously reduced by increasing the thermal resistance between the physics package and the environment. **Figure 26** shows a CSAC physics package that consumes <10 mW of power at an ambient temperature of 25°C to heat the cell (Lutwak *et al.* 2004). The heat conduction has been reduced to 13 μW K^{-1} by suspending the physics package on a thin web of strained polyimide support tethers. Electrically conductive leads composed of gold and platinum are deposited on top with a titanium adhesive layer to supply the heating current.

Convection is minimized by vacuum packaging. Immersion has been suggested as a lower-cost alternative in some materials of low thermal conductivity. A different approach for a MEMS clock physics package has been proposed by Youngner *et al.* (2005), and also includes a thermal suspension system (**Figure 27**).

One of the major challenges in the thermal management is the requirement to maintain temperature control better than 100 mK over a wide range of ambient temperatures (−40 to +70°C) with a small power budget. This is further complicated by the heat dissipated by the VCSEL (Kitching *et al.* 2004). One solution can be a MEMS thermal conduction switch that can change the thermal resistance between the physics package and the environment (Laws *et al.* 2005). A schematic of a physics package that implements such a thermal switch is shown in **Figure 28**.

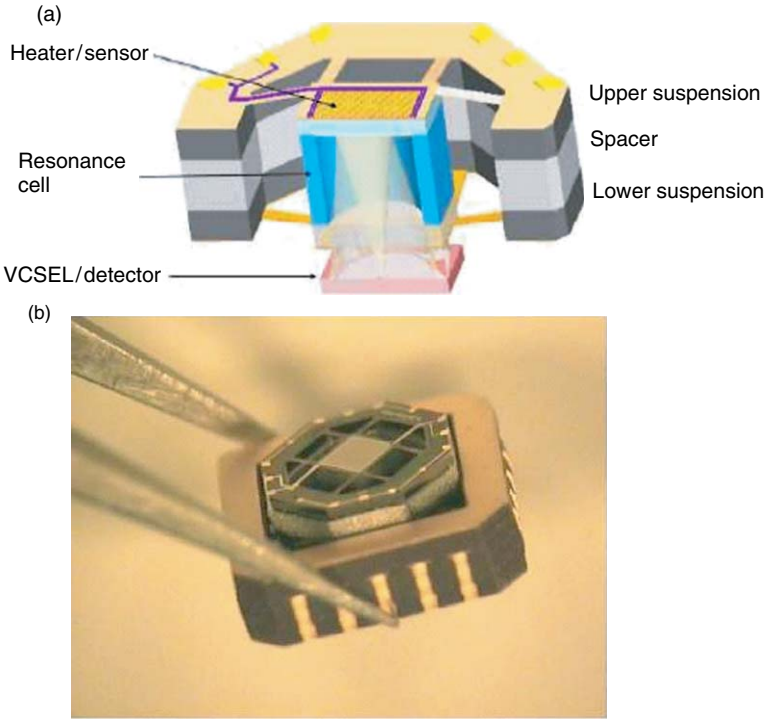

Figure 26 (a) Cutaway view and (b) photograph of a low-power chip-scale atomic clock (CSAC) physics package. (Source: Lutwak R, Deng J, Riley W, Varghese M, Leblanc J, Tepolt G, M.Mescher, Serkland D K, Geib K M, Peake G M 2004 The chip-scale atomic clock – Low-power physics package. *36th Annual Precise Time and Time Interval (PTTI) Meeting*, Washington, DC, USA, pp. 1–14. Honeywell permission.)

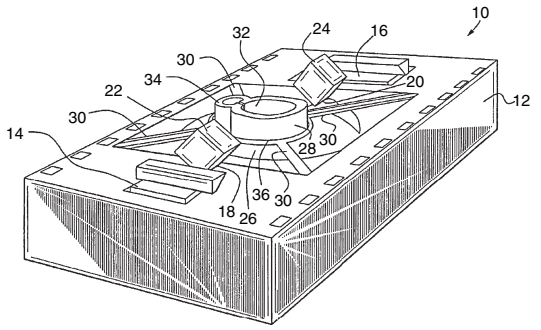

Figure 27 Schematic of a chip-scale atomic clock (CSAC) physics package (10) design including: substrate (12), light source (14), light detector (16), grooves (18, 20), optical processors (22, 24), cavity (26), vapor cell (28, 32, 44), bridge (30), and heater (36). (Source: Youngner D W, Detry J F, Zook J D 2005 MEMS frequency standard for devices such as atomic clocks. *US PTO* 6 900 702 B2.)

3.18.3 Performance

3.18.3.1 Introduction

The long-term goal for most CSAC projects, set by DARPA, is to reach a frequency instability below 10^{-11} at 1 h of integration in a 1 cm^3 package consuming <30 mW of power. Therefore, most CSACs have been characterized mostly by these three specifications: frequency stability at times <1 h, size, and power consumption. Nevertheless, for many applications, other specifications, such as frequency stability at times longer than a week, accuracy, acceleration sensitivity, magnetic field sensitivity, lifetime, no unlocks for long durations, might be at least as important. At the same time, which specifications will be set for the CSAC will strongly depend on the application. In the following sections, we nevertheless focus mostly on the three specifications set by DARPA.

3.18.3.2 Frequency Stability

3.18.3.2.1 Introduction

Atomic clocks are often characterized by their Allan deviation $\sigma_y(\tau)$ (for a review, see Allan 1987), which is a measure of the fractional frequency stability as a function of averaging time τ. Over short averaging times, the stability of many atomic clocks is characterized by white frequency noise. For this type of noise, the Allan deviation decreases as $\tau^{-1/2}$ (**Figure 29**, light gray dots) and can be expressed in

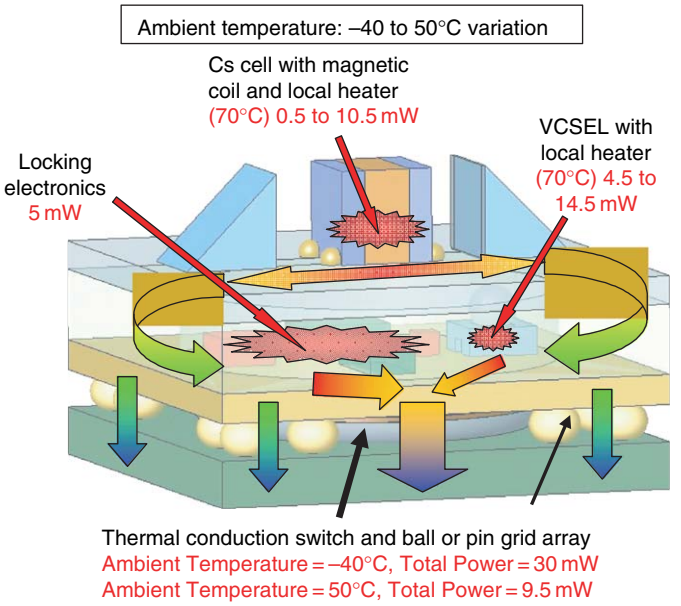

Figure 28 Illustration of heat transfer path through a chip-scale atomic clock (CSAC) design using a thermal conduction switch to reduce overall power consumption. Heat rates are estimated to meet clock power requirements of <30 mW. Radiation and conduction/convection are ignored. (Courtesy of V. Bright.)

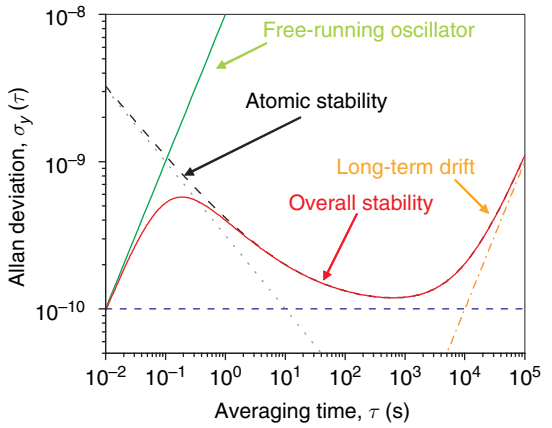

Figure 29 Fractional frequency stability: free-running oscillator (dashed green line), supported by the atoms (dashed black line), when locked to the atomic resonance. The atomic stability here is determined by white frequency noise (light gray dots), flicker noise floor (dashed blue dots), and frequency drift (orange dashes).

terms of signal-to-noise ratio S_{CPT}/N and resonance quality factor Q (Vanier 2001)

$$\sigma_y(\tau) = \frac{\chi}{QS_{\mathrm{CPT}}/N}\frac{1}{\sqrt{\tau}} \qquad [4]$$

Here, $Q = \nu_0/\Delta\nu_{\mathrm{CPT}}$ is defined as the ratio of resonance frequency over linewidth and χ is a parameter of the order of unity related to the method of interrogation. It is desirable to have a high signal-to-noise ratio and a narrow linewidth in order to reach good frequency stability. The fractional frequency stability of these clocks improves over measurement time until it reaches the flicker noise floor, $\sigma_y(\tau) \propto \mathrm{const}$ (**Figure 29**, blue dashes), or until the frequency starts drifting, $\sigma_y(\tau) \propto \tau$ (dashed orange dots). These drifts are usually caused by environmental variations that change the clock frequency over time. A typical Allan deviation determined by the atoms is shown in **Figure 29** (black dashes). In a passive CPT clock, an LO generates a signal close to the clock frequency. The physics package uses this signal as its input to create an output signal that carries information about the frequency difference between the LO frequency and the atomic frequency. This information can then be used to tune the LO frequency so that it always coincides with the one of the atoms (for a review on CPT clocks, see, e.g., Vanier 2005). Thus, the stability of the clock is determined by the LO stability at times shorter than the inverse loop bandwidth, and by the atoms at longer times (**Figure 29**, red line).

For a CSAC, the frequency stability can be predicted in the photon shot-noise limit to be on the order of $\sim 2 \times 10^{-13}/\tau^{1/2}$ for a 1-mm^3 cell and

typical experimental parameters (Vanier *et al.* 2003d). Unfortunately, in an experimental setup, this stability has not been reached, since other noise sources are dominant and the signals are small. For VCSELs, laser amplitude noise and laser frequency noise play a major role. Frequency noise gets converted into amplitude fluctuations through the atomic resonances (Camparo and Buell 1997, Coffer *et al.* 2002). In most CSACs, the VCSEL is locked to the center of a resonance, so that this effect is drastically reduced in comparison to when locked to the side of the resonance (Kitching *et al.* 2001b), but it nevertheless remains significant. Here it can be advantageous to use a high buffer gas pressure where the optical lines are very broad and have a shallow FM–AM conversion slope (Camparo 1998a). Furthermore, in some VCSELs, mode-competition noise (Kaiser *et al.* 2002, Mukaihara *et al.* 1995b) between different polarization modes causes large contributions to the noise on the detector, especially when transformed into amplitude noise by a polarizer. All of these noise sources reduce the frequency stability, so that the best short-term stability reported to date in a CSAC physics package is $4 \times 10^{-11}/\tau^{1/2}$ in a 1-mm^3 cell (Knappe *et al.* 2005b).

Besides the effects that limit the short-term stability of the CSAC, frequency shifts and line shape asymmetries can cause major problems at longer averaging times. They can result from magnetic fields, buffer gas pressure, temperature, light shifts, acceleration, or RF power. It is therefore critical to control these parameters carefully or to find a measurement scheme that reduces the frequency sensitivity to changes in these parameters.

While for many primary frequency standards the absolute clock frequency is critical (Quinn 2005), for most applications of chip-scale clocks this value is of minor interest, as long as it can be calibrated. Nevertheless, it is of great importance that the clock frequency does not change over time, i.e., it needs good stability, but not necessarily good accuracy.

3.18.3.2.2 Short-term frequency stability

The first CSAC physics package demonstrated used the D_2 line of cesium (Knappe *et al.* 2004b). Its short-term frequency stability of $6 \times 10^{-10}/\tau^{1/2}$ was limited by a CPT resonance contrast of 0.9% and a CPT linewidth of 7 kHz. The package had a volume of 9.5 mm^3 and required 75 mW of power at an external baseplate temperature of 46°C. The power budget did not include heating of the laser. A plot of the Allan deviation for this CSAC physics package is shown in **Figure 30** (black squares).

It has been shown for cesium (Lutwak *et al.* 2003) as well as for rubidium (Stähler *et al.* 2002) that the CPT resonance contrast is much higher on the D_1 line than on the D_2 line. The first CSAC physics package using the D_1 line of ^{87}Rb was demonstrated shortly after (Knappe *et al.* 2005b). The short-term frequency instability was $4 \times 10^{-11}/\tau^{1/2}$, the best short-term frequency instability reported so far for this simplest type of CPT CSAC with a 1-mm^3 vapor cell. A plot of the Allan deviation can be found in **Figure 30** (red dots). The improvement can be attributed to a higher CPT resonance contrast of 4.6% as well as to fewer Zeeman sublevels in ^{87}Rb when compared to Cs. Finally, a CSAC physics package using the D_1 line of cesium has also been presented with a short-term frequency instability of $1.4 \times 10^{-10}/\tau^{1/2}$ (Lutwak *et al.* 2005).

When the physics package is integrated with a miniature LO, the performance of the CSAC can change dramatically. In order to reach large tuning ranges, the tunability of the LOs often needs to be around 1 MHz V^{-1}, making them very sensitive to voltage fluctuations on the tuning input. Also, most small low-power LOs have phase noise around −40 dBc at 100 Hz at best, which puts tight constraints on the control system. Nevertheless, short-term stabilities of $2.4 \times 10^{-10}/\tau^{1/2}$ have been demonstrated with an integrated low-power LO physics package design (Brannon

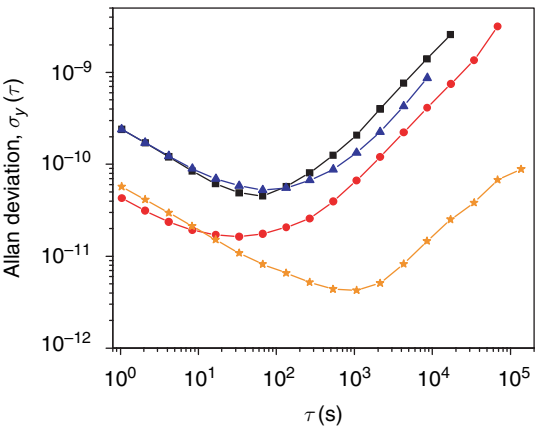

Figure 30 Fractional frequency stability as a function of averaging time for a Cs D_2 chip-scale atomic clock (CSAC) physics package (black squares), ^{87}Rb D_1 CSAC physics package (red dots), CSAC physics package with integrated local oscillator (LO) (blue triangles), and 1-mm^3 ^{87}Rb vapor cell (orange stars).

et al. 2006b) (**Figure 30**, blue triangles). Disciplining the VCO by the use of small control electronics can be challenging, as higher servo bandwidths are desired when compared to oscillators with better phase noise. This is worsened by the fact that several servo loops have to be controlled simultaneously. It has been shown that an integrated CSAC (matchbox size) can nevertheless support a fractional frequency stability of $6 \times 10^{-10}/\tau^{1/2}$ (Lutwak *et al.* 2005).

3.18.3.2.3 Long-term frequency stability

Until now, we have discussed only frequency stability for integration times <100 s. **Figure 30** shows that frequency drifts determine the stability of these CSACs at integration times >100–1000 s. Most drift is directly or indirectly caused by temperature fluctuations. The stabilities presented here were measured in a laboratory environment. It has been shown that under such conditions, MEMS cells can support frequency stabilities below 1×10^{-11} at 1 h and below 1×10^{-10} at one day (Knappe *et al.* 2005a) (see orange stars in **Figure 30**). Nevertheless, it can be expected that in a real-world environment, the frequency stabilities of these CSACs will degrade severely if the shifts are not addressed. In the following, we discuss different parameters that influence the long-term stability.

3.18.3.2.3.(i) Buffer gas pressure

As described in Section 3.18.1.4, a buffer gas is used to narrow the CPT linewidth. At the same time it shifts the hyperfine frequency. This shift is temperature-dependent. A standard way to reduce the temperature coefficient of the clock frequency in commercial optically pumped devices is to use combinations of buffer gases that shift in opposite directions (Arditi and Carver 1961, Vanier *et al.* 1982). The same technique works well for CPT clocks (Knappe *et al.* 2001). However, in small devices, the residual temperature coefficient is proportional to the total buffer gas pressure. Because the pressure in most approaches is nearly an order of magnitude higher than in centimeter-sized devices, coefficients worsen accordingly. Furthermore, the buffer gas combinations are harder to control in microfabricated cells, because the anodic bonding process with its high temperatures can create residual gases inside the cell. Therefore, the cell temperature has to be stabilized precisely. It has been shown, however, that the temperature stability of the cell (as well as the VCSEL) can be improved when direct absorption signals from the atoms are used to determine the temperatures, instead of temperature sensors in the vicinity of the cell (or VCSEL) (Gerginov *et al.* 2006b).

3.18.3.2.3.(ii) Light shifts

Compared to optically pumped clocks, light shifts can be reduced in CPT, because of the ability to create a more symmetric system (Levi *et al.* 2000, Orriols 1979, Vanier *et al.* 1998). Nevertheless, the frequency stability of most CSACs is still limited by light shifts at long averaging periods.

VCSELs have frequency tunabilities of roughly $300\,\mathrm{GHz\,K^{-1}}$ (see Section 3.18.3.2.3). Therefore, it is essential to stabilize their temperatures precisely. This is usually done with small temperature sensors, e.g., thermistors close to the VCSEL die. When temperature gradients between the sensor and the die change the VCSEL junction temperature, for example, due to ambient temperature fluctuations, its output frequency changes. The frequency servo then changes the DC current of VCSEL to pull it back onto resonance, but the output power as well as the VCSEL impedance, that is, modulation index of the light field, is usually different (Gerginov *et al.* 2006b). This in turn generally changes the clock frequency through altered light shifts (Arditi and Carver 1961, Barrat and Cohen-Tannoudji 1961, Mathur *et al.* 1968). It has been shown in a large cell (Levi *et al.* 2000, Vanier *et al.* 1999, Zhu and Cutler 2000, 2001) as well as in a CSAC (Gerginov *et al.* 2006b) that when the right RF modulation index is chosen, the total light shift from the laser carrier and all other sidebands vanishes. A similar technique has been implemented in a microwave clock as well (Affolderbach *et al.* 2006). Furthermore, an additional servo loop can be used to lock the RF power to this point, where no light shifts are present (Shah *et al.* 2006a).

3.18.3.2.3.(iii) Other frequency shifts

The field of MEMS clocks is very young when compared to that of lamp-pumped Rb standards. The use of new materials and components raises many uncertainties onto the performance of these new devices. Careful characterization and engineering over the coming years will be required to turn the current prototypes into reliable off-the shelf devices. In the following, a few of these parameters are summarized.

An important frequency shift is the RF output power of the LO. In an in-field environment where temperatures and coupling to metal objects can change dramatically, the RF power of the VCO is difficult to control. The clock frequency depends critically on the

power distributed over all modulation sidebands through light shifts. The modulation index therefore needs to be stabilized. Two methods have been demonstrated to do this. In a CSAC, the RF power can be locked to the point where the power in the first-order sidebands is maximized (Gerginov *et al.* 2006b). In a table-top CPT setup, the RF power is locked to the point where the total light shift vanishes (Shah *et al.* 2006a). Furthermore, the slow modulation of the LO frequency used for phase-sensitive detection of the CPT resonance can lead to shifts in the clock frequency (Phillips *et al.* 2006).

As mentioned in Section 3.18.2.2.6, the clock frequency is shifted as a function of total magnetic field. At the time of writing (2006), no measurements that characterize the residual shifts that occur after packaging and shielding have been published.

Since MEMS clocks are supposed to work in portable devices, acceleration insensitivity is of importance, and CSACs have not yet been characterized in this way. Nevertheless, two LOs have been specified with 0.2–0.3 ppm g^{-1} at 10 Hz (Brannon *et al.* 2006b) for these clocks.

Furthermore, in optically pumped clocks with their glass-blown vapor cells, diffusion of gases such as helium through the glass walls can cause problems (Bloch *et al.* 2000, Camparo *et al.* 2005). Chip-scale cells have not been characterized in this respect. But thin glass windows and new bonding mechanisms can be of concern. And finally, the reliability of the VCSELs with unknown behaviors in CSACs due to aging, sparks, radiation, etc., is yet to be determined. Nevertheless, initial performance results are encouraging, given the very short development time and the lack of any serious engineering.

3.18.3.3 Power Consumption

The power consumed by the first CSAC physics packages, which had essentially no thermal shielding, was 200 mW (Knappe *et al.* 2004b, 2005b). Nevertheless, their thermal properties have been modeled and characterized (Kitching *et al.* 2004). As discussed in Section 3.18.2.5, the main portion of the power was expended in heating the cell and the VCSEL. Therefore, it can be favorable to use cesium rather than rubidium, because of a higher vapor pressure. It has been convincingly demonstrated that it is possible to reduce heat conduction to below 13 μW K^{-1} in a CSAC physics package and therefore to heat a CSAC cell of volume 8.5 mm^3 to 75°C at an ambient temperature of 25°C with only ~6 mW of power (Lutwak *et al.* 2004). Since Rb has a slightly lower vapor pressure, with the same setup, it would require ~8.5 mW to reach a similar density at 90°C.

As discussed in Section 3.18.2.3, a VCO at 3.417 GHz is required for ^{87}Rb with an output power of at least −6 dBm and at 4.596 GHz for Cs with an output power of ~0 dBm. Two of these have been successfully demonstrated, requiring 2.1 mW (Brannon *et al.* 2006a) and 7.6–10 mW (Römisch and Lutwak 2006) for ^{87}Rb and Cs, respectively.

Control electronics have been developed using microcontrollers, resulting in packages around 10 cm^3 in size (see Section 3.18.2.4). For these, power budgets below 30 mW have been reported (Lutwak *et al.* 2005). For a complete miniature atomic clock package, including three such components, a total power budget of 108 mW was quoted (Lutwak *et al.* 2005). This included a commercial 4.6-GHz VCO. When this is replaced by one of the small low-power VCOs described here, the power budget is expected to be reduced further.

Finally, if an output frequency of 10 MHz is required, the odd output frequency in the gigahertz range has to be converted down. This can be done either by phase-locking a higher-power microwave VCO to a 10-MHz VCO (similar to **Figure 25**) or by adding an external frequency divider. The latter could consist of a fractional-*N* divider locked to a TCXO, for example. Such a device, as depicted in **Figure 31**, has been built on the same footprint as the

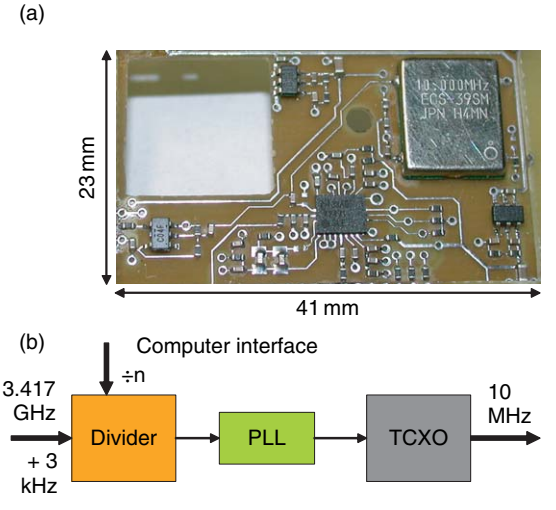

Figure 31 Photograph (a) and schematic (b) of a frequency divider for chip-scale atomic clock (CSAC). The fractional-*n* divider chip is programmed to divide 3.417 GHz down to 10 MHz. The output signal is then phase-locked to a 10-MHz temperature-compensated quartz crystal oscillators (TCXO).

NIST MEMS clock and consumes <30 mW of power (Waltman 2006). The TCXO acts as a cleanup oscillator that filters the modulation sidebands off the signal and reduces the phase noise at higher frequencies.

3.18.3.4 Size

The smallest CSAC physics package so far that consists of VCSEL, optics, cell, and photodiode has been demonstrated by Lutwak *et al.* (2005). It has a volume of 10 mm^3 without packaging. A picture is shown in **Figure 26**. The VCSEL is surrounded by a narrowband photodetector grown on the same substrate. After the diverging beam from the laser passes is attenuated and circularly polarized, it passes through the cesium vapor cell. Then it is retroreflected back through the cell onto the photodetector surrounding the VCSEL. The temperatures of the VCSEL and detector are stabilized together, so that their passbands are tuned simultaneously. When thermal packaging is included, it has a volume of ~1 cm^3. The smallest LO demonstrated to work with a CSAC physics package has a volume of ~0.15 cm^3 (Brannon *et al.* 2006a).

Finally, when integrating the control electronics with physics package and LO, a total volume of 10 cm^3 has been demonstrated (Lutwak *et al.* 2005). While this size is comparable to that of the smallest CPT vapor cell clock based on conventional technology (Vanier *et al.* 2004, 2005), its power is reduced by a factor of 5. With the CSAC technology demonstrated so far it is possible to reduce the volume of the control electronics to below 0.5 cm^3, allowing the CSACs to have volumes of around 1 cm^3.

3.18.4 Advanced Techniques

3.18.4.1 Introduction

Until now, we have mainly discussed the simplest approach to a CSAC: one VCSEL, one beam, one cell, and one photodetector, all in a straight line. The CPT resonance excited in this way couples the $m_F = 0$ ground states to either the $m_F = +1$ or the $m_F = -1$ excited state with circularly polarized light. The short-term performance of the CPT clock can then be characterized by the resonance contrast, defined as the amplitude of the CPT resonance over the background, the resonance width, and the noise. The performance at longer times is determined mostly by frequency shifts induced through time-dependent changes of external parameters. The progress of the CSAC project has triggered various new approaches that can potentially improve the clock performance. In the following section some of these more advanced techniques are discussed.

3.18.4.2 Resonance Contrast

It has been mentioned earlier that the resonance contrast (as well as the CPT width) is more favorable on the D_1 line as compared to the D_2 line. This has been experimentally (and theoretically) demonstrated for rubidium (Stähler *et al.* 2002) as well as for cesium (Lutwak *et al.* 2003). However, when using circularly polarized light on the D_1 line, a new problem arises due to the existence of a second dark state, the so-called stretched state or incoherent trapping state $|S_{1/2}: F = 2I + 1, m_F = \pm F\rangle$. This open system has been successfully modeled theoretically through a system with four levels, or with three levels and a trap (Vanier *et al.* 2003b). **Figure 32(a)** shows the level structure of the D_1 line of ^{87}Rb as an example. As the light intensity is increased, more atoms are pumped into the CPT state, but at the same time, more atoms are also lost into the stretched state, and the fraction of the atoms in the dark state drops again. **Figure 33(a)** shows the CPT absorption contrast (CPT amplitude divided by Doppler absorption) as a function of light intensity for a closed system (black) and a more realistic open system (red). **Figure 33(b)** and **33(c)** shows the CPT resonance width and the CPT resonance amplitude calculated for the same two systems, respectively (Shah *et al.* 2004).

A few different methods have been demonstrated in the past years to circumvent this problem of pumping. The simplest way would be to use linearly polarized light, as a combination of right-hand and left-hand circularly polarized light simultaneously. However, it has been shown (Wynands and Nagel 1999) that this forms a closed-loop system (Korsunsky *et al.* 1999, Kosachiov *et al.* 1992, Lukin *et al.* 1999, Shahriar and Hemmer 1990) on the 0–0 levels, which destructively interferes. A coherent dark state can be formed only in atoms that can couple simultaneously to more than one excited state from one pair of ground states (as in **Figure 32(b)**), if the following two conditions are fulfilled (Buckle *et al.* 1986, Kosachiov *et al.* 1991, 1992, Maichen *et al.* 1995, 1996):

$$\frac{g_1}{g_2} = \frac{g_3}{g_4} \quad \text{and} \quad \varphi_1 + \varphi_2 + \varphi_3 + \varphi_4 = 0 \qquad [5]$$

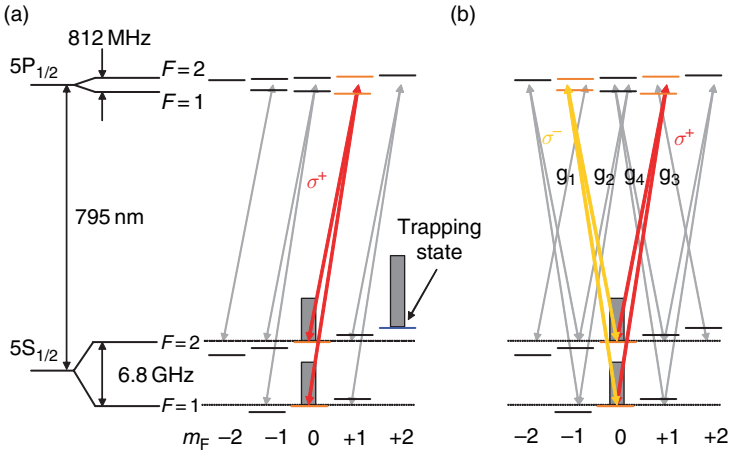

Figure 32 Atomic levels of the ^{87}Rb D_1 line. The levels involved in the coherent population trapping (CPT) coherence are shown in orange. (a) In this open system the circularly polarized light fields (red) optically pump atoms into the trapping state shown in blue. The gray columns indicate the atomic population distribution. (b) Adding an additional pair of light fields (yellow) with opposite circular polarization can eliminate the trapping state. The four optical transitions are coupled by the light fields E_j (with phases φ_j) and Rabi frequencies $g_j, j \in \{1–4\}$.

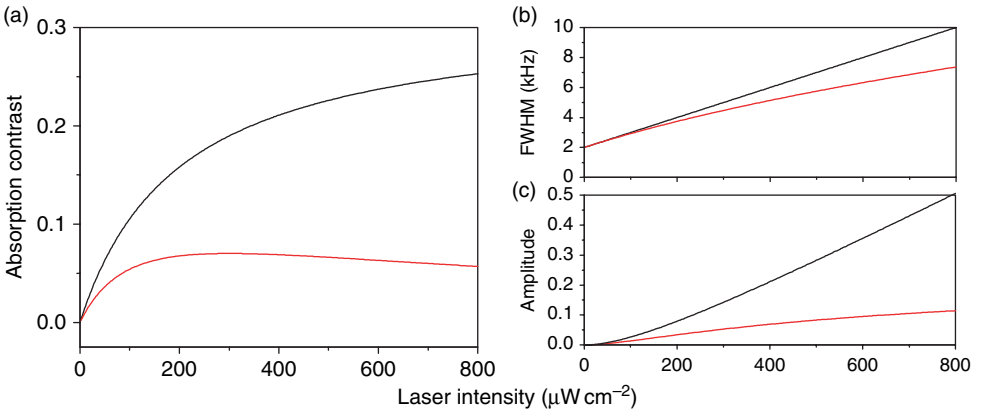

Figure 33 Calculations for a symmetric open (red) and a closed (black) Λ-system. Coherent population trapping (CPT) resonance absorption (a) contrast, (b) width, and (c) amplitude are plotted as a function of laser intensity. (Source: Shah V, Knappe S, Hollberg L, Kitching J 2004 On open Λ systems and the stability of coherent population trapping devices. Unpublished.)

Here, g_j is the Rabi frequency and φ_j is the phase associated with the jth light field, $j \in \{1–4\}$, as shown in **Figure 32(b)**. For linearly polarized light, on the two $m_F = 0$ ground-state levels $g_1/g_2 = -g_3/g_4$ so that no CPT resonance can be observed.

It has been shown that right-hand and left-hand circularly polarized light can nevertheless be used simultaneously to couple the same pair of ground states, if one beam is delayed by half a microwave wavelength (Affolderbach *et al.* 2002, Alzetta *et al.* 1999). This shifts the relative phase of one beam by π with respect to the other. Jau *et al.* (2004a) have nicely demonstrated that this can be used to increase the contrast of the CPT resonance by eliminating the incoherent trapping state. This transforms the open system back to a closed system (see **Figure 33**). A similar way to create this phase delay is by reflecting the circularly polarized beam back onto itself with opposite circular polarization and by placing the cell a quarter of a microwave wavelength away from the mirror (Affolderbach *et al.* 2002, Alzetta *et al.* 1999, Kargapoltsev *et al.* 2004, Taichenachev *et al.* 2004). It is difficult to integrate either of these methods into a small CSAC due to the delay of half a microwave

wavelength, which is 2 cm for ^{87}Rb. The trapping of atoms in the stretched state can also be circumvented by using two phase-locked single-frequency laser beams with linear orthogonal polarization separated in frequency by the ground-state splitting frequency (Nagel 1999, Zanon *et al.* 2005), but this is not convenient for a compact portable device. One way to implement these ideas into a CSAC physics package has been demonstrated by Shah *et al.* (2006b). They used two VCSEL dies with orthogonal polarizations. The linear light fields were converted into orthogonally circularly polarized fields before entering a microfabricated ^{87}Rb vapor cell. Instead of delaying one optical beam, the microwave phase was delayed by π.

The goal of these very similar techniques is to enhance the resonance contrast and therefore improve the frequency stability of the clock. However, in most cases, the clock is operated at a light intensity where the linewidth is roughly twice the zero-intensity linewidth only (for **Figure 33** this roughly correspond to $200\,\mu W\,cm^{-2}$). Since the linewidths for the open system and the closed system are roughly the same, it would correspond to an increase in CPT resonance amplitude roughly by a factor of 2. Assuming that the noise remains the same, it is questionable whether the more complicated setup justifies an increase in the frequency stability by a factor of 2 (Shah *et al.* 2006b), unless there is another advantage gained at the same time. Especially so, if the CPT amplitude can also be increased by a higher atomic density, until spin-exchange broadening counteracts the gain in frequency stability.

A different way to increase the contrast of CPT resonances has been investigated by Zhu (2003). Here, only a small amount of opposite circularly polarized light is added (without phase delay). While the medium becomes more transparent under CPT conditions for the strong polarization component, the weak one experiences enhanced absorption. Both components acquire opposite phase shifts. A polarization analyzer system is then adjusted such that only a small fraction of the strong polarization component is transmitted, and the relative phase delay in both polarization components is optimized to give a symmetric CPT signal with contrasts above 20%.

When limited to one laser, parallel linear polarizations can be used to couple a coherence between the ground states $|F,\ m_F=\pm1\rangle$ and $|F+1,\ m_F=\Upsilon1\rangle$ (Kazakov *et al.* 2005b, Knappe *et al.* 1999, Taichenachev *et al.* 2005, Zhu 2004). These resonances are also insensitive to magnetic fields in first order, but split at higher fields due to the contribution of the nuclear magnetic moment. Since this is a coherence between two states with $\Delta m_F=\pm2$, it is suppressed at higher buffer gas pressures when the excited-state hyperfine structure is unresolved (Wynands and Nagel 1999).

A different way to accumulate atomic population in the 0–0 states has been demonstrated for optically pumped clocks (Bhaskar 1995) by using a series of microwave pulses. In a similar manner, a population can be optically pumped into one of the $m_F=0$ states using π-polarized light that is resonant with the transition $|F\rangle\rightarrow|F\rangle$ (Kazakov *et al.* 2005a, Shah *et al.* 2004), where the transition between the $m_F=0$ states is forbidden. The atoms will then accumulate in this state, while they are probed by circularly polarized light under CPT conditions. This technique also requires the excited-state hyperfine structure to be resolved for efficient pumping and two light fields from orthogonal directions.

3.18.4.3 Buffer Gas

We have seen in Section 3.18.2.3 that the CPT linewidth has a minimum at an optimum buffer gas pressure. From **Figure 5** it can be seen that for a 1-mm cell of ^{87}Rb and nitrogen, this optimum pressure is several atmospheres. At the same time, the buffer gas broadens the optical $S\rightarrow P$ transition. For a frequency-modulated light field, the CPT contrast dramatically reduces when this optical width approaches the ground-state splitting (Arimondo 1996a, Nikonov *et al.* 1994, Post *et al.* 2005), because the carrier and second-order light fields become resonant. They can cause single-photon transitions pumping atoms out of the dark state. They fulfill the dark-state condition as well, but their relative phase differs from the phase between the first-order sidebands. CPT resonances have nevertheless been observed in small cells with several atmospheres of buffer gas, where the ground states were unresolved, when the laser was amplitude-modulated with a $LiNbO_3$ Mach–Zehnder modulator (Jau *et al.* 2004a, Post *et al.* 2005). In most CSACs though, the buffer gas pressure is chosen such that the ground-state hyperfine structure is still resolved, and the linewidth is typically limited by wall collisions.

In table-top systems, antirelaxation wall-coated cells have proven to exhibit extremely narrow linewidths (Bouchiat and Brossel 1966, Robinson *et al.* 1958). Alkenes (C_nH_{2n+2}), such as tetracontane or paraflint, as well as silanes gave good results for Rb

and Cs Zeeman and hyperfine transitions (Budker *et al.* 2005, Frueholz *et al.* 1983, Risley *et al.* 1980, Robinson and Johnson 1982). However, accommodation coefficients (a measure of the average number of wall collisions before decoherence) for hyperfine transitions are found to be worse than for Zeeman transitions by about an order of magnitude (Robinson and Johnson 1982). Nevertheless, it could be advantageous to use wall coatings for small clocks, possibly in combination with low pressures of buffer gases. Advantages could include a reduced temperature dependence (Section 3.18.3.2.3.1), narrower linewidth, lower operating temperatures, or resolved excited-state hyperfine structure. The latter could allow for other interrogation schemes that couple ground states with $\Delta m_F = \pm 2$ (Kazakov *et al.* 2005b, Knappe *et al.* 1999, Taichenachev *et al.* 2005, Zhu 2004), which are suppressed at higher buffer gas pressures (Wynands and Nagel 1999). Research is progressing in this area to find new wall-coating materials that are amenable to microfabrication of vapor cells and that can withstand higher bonding and operating temperatures.

3.18.4.4 Spin Exchange

As cell length decreases, the alkali vapor density usually increases to maintain sufficient absorption through the cell (typically ~50%). At these densities, another broadening mechanism starts to dominate the CPT linewidth, caused by collisions between alkali atoms (Happer 1972, Walker and Happer 1997), as mentioned in Section 3.18.1.3. These so-called spin-exchange collisions conserve the total angular momentum of the pair of alkali atoms. By pumping the atoms into the stretched state with maximum angular momentum, the linewidth of the microwave resonance can be dramatically reduced (Jau *et al.* 2003, 2004b). However, this resonance frequency is strongly dependent on the magnetic field ($21\,\mathrm{kHz}\,\mu\mathrm{T}^{-1}$ for ^{87}Rb and $25\,\mathrm{kHz}\,\mu\mathrm{T}^{-1}$ for Cs), which has to be precisely controlled (see Section 3.18.5.2).

3.18.4.5 Noise Suppression

Most of the noise on the CPT resonance is from the VCSEL through frequency and/or intensity fluctuations (see Section 3.18.2.2.2). When locked to the top of the atomic resonance line, these contributions can be comparable to that of the photon shot noise (Kitching *et al.* 2001c). Furthermore, polarization mode-competition noise can be severe for some VCSELs, but negligible for others. They can be converted into intensity fluctuations when using a polarizer. To reduce the influence of laser-induced noise, two laser beams can be passed through the same vapor cell, inhibiting the same laser noise but different CPT signals.

Gerginov *et al.* (2006a) demonstrated a simple setup in a microfabricated vapor cell of area $2\,\mathrm{mm} \times 1\,\mathrm{mm}$ using two parallel beams, one with circular polarization and another with linear polarization. For the reasons described in Section 3.18.4.2, only the circularly polarized beam causes a CPT resonance. Subtracting the two photodiode signals cancels most of the laser-induced noise, but leaves the full CPT signal. It does not cancel the shot noise, but rather doubles it, so this technique improves the clock stability only if dominated by laser noise, e.g., when locked to the side of the resonance line. Additional noise caused by the CPT resonance itself cannot be reduced in this setup.

Additional noise reduction might be possible, however, with a differential detection technique, where the two beams have orthogonal circular polarization and propagate parallelly through the same region of the cell (Rosenbluh *et al.* 2006) in a similar manner as described in Section 3.18.4.2. The relative phase delay between the two beams here is $\pi/2$, as compared to π previously. This causes the CPT resonance not to have an absorptive Lorentzian lineshape, but rather a combination of absorptive and dispersive Lorentzians. The CPT signal in both beams has an opposite sign for the dispersive part of the signal, so that the difference signal is dispersive in shape. Because the laser noise on both signals is similar, it cancels. A noise suppression of 20 dB has been measured in a table-top setup.

3.18.5 Other CSAC Approaches

3.18.5.1 Introduction

Until now we have primarily discussed passive CSACs based on locking a VCO to a CPT transmission signal. There has been a series of other approaches, of which a few are introduced in the following sections. Unfortunately, not much has been published on these.

3.18.5.2 End-State CSAC

It has been mentioned in Section 3.18.4.4 that microwave resonance broadening due to spin-exchange

collisions between the alkali atoms can be largely reduced when the atoms are pumped into the stretched state (Jau *et al.* 2004b). This can lead to much narrower resonance lines and better stability of CSACs. A gain in sensitivity can be achieved by increasing the cell temperature into a region where spin-exchange collisions usually dominate the linewidth broadening, e.g., high buffer gas pressures. In general, this method works with CPT and microwave interrogation, but for CPT, a second laser beam would be required for optical pumping. Therefore, the scheme was implemented using microwave interrogation (Jau *et al.* 2006).

Since the end-state resonance frequency is very sensitive to magnetic fields, the magnetic field has to be stabilized precisely. This can be done by measuring the Lamor frequency and implementing an additional servo to stabilize the magnetic field (Jau *et al.* 2006) or by alternating between the two opposite stretched states to find the unshifted mean frequency. Furthermore, by choosing the right laser detuning, light shifts have been reduced simultaneously (Jau *et al.* 2006). Potentially, better stabilities could also be reached in microwave-interrogated CSACs, because no high FM is required and therefore lower noise VCSELs might be used.

3.18.5.3 Nanomechanically Regulated CSAC

An RF-interrogated CSAC that uses a mechanical motion to modulate the magnetic field at the location of the ^{87}Rb atoms has been proposed. This oscillation can be induced by using micromechanical choppers that attenuate the magnetic field depending on their position, oscillating at 6.8 GHz, for example (Lee *et al.* 2004).

Even though coupling of alkali atoms to the mechanical oscillation of a MEMS structure has not been demonstrated at gigahertz frequencies yet, it has been shown that double-resonance transitions can occur in ^{87}Rb atoms inside a MEMS vapor cell by using a magnetic cantilever oscillating at 15 kHz (Wang *et al.* 2006).

3.18.5.4 CPT Maser

Under CPT conditions, a coherence is created between the two ground states, oscillating at the difference frequency between them. As a result, the amount of light absorbed by the alkali vapor decreases. At the same time the oscillating magnetization can be detected through stimulated emission in a cavity (Vanier *et al.* 1998). This will happen when a microwave cavity surrounding the cell is tuned to the same ground-state hyperfine frequency. This signal can be used to lock the LO, which generates the modulation on the laser, by synchronous detection (**Figure 34**). While laser noise is not transmitted directly to the microwave signal, a change in sideband intensities and detunings can nevertheless change the output frequency through variations of the ground-state coherence (Godone *et al.* 2000, Levi *et al.* 2000). Using a method similar to the simple CPT clock, the modulation index can be chosen such that the overall light shift is reduced (Vanier *et al.* 1999).

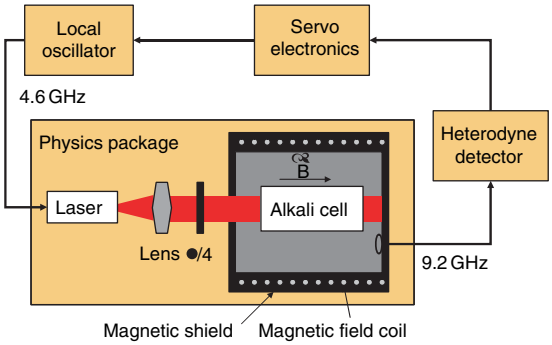

Figure 34 Conceptual setup of a coherent population trapping (CPT) maser.

Furthermore, effects such as cavity pulling, that is, detuning of the cavity with respect to the resonance and shifts due to finite microwave power and phase of the emitted field, can affect the frequency stability of the maser (Godone *et al.* 2000). Even though better stabilities can be potentially reached with a CPT maser (Vanier *et al.* 2003a), the size and the complication of the microwave cavity have prevented it from being used in chip-scale clocks.

3.18.5.5 Raman Oscillator

We have seen in Sections 3.18.1.3 and 3.18.1.4 that the ground-state coherence induced under CPT conditions can be detected in different ways: as a change in the transmission (or fluorescence) or through stimulated microwave emission. Yet another way of detecting the resonance is by detecting the light on a fast photodetector and by detecting the beat signal at the ground-state splitting frequency, e.g., 6.8 GHz for ^{87}Rb (Vukičević *et al.* 2000). No modulation of the VCSEL is necessary to detect this signal, since the second light field is created through stimulated

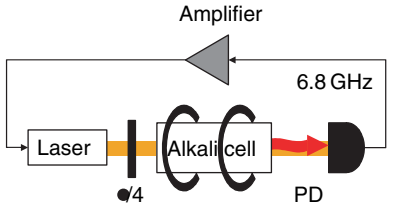

Figure 35 Closed-loop Raman oscillator. The 6.8-GHz signal is fed back to the injection current of the laser.

Raman scattering. However, the linewidth of this resonance can be fairly large in order to achieve enough Raman gain to detect the RF signal, and strong Stark shifts due to high laser intensities can limit the clock stability. This stimulated Raman oscillator design can provide better frequency insensitivity to accelerations when compared to the passive DC CPT clock, because the signal is derived from a purely atomic process.

To increase the signal-to-noise ratio, and allow for lower light intensity, a feedback loop can be included that feeds the amplified 6.8-GHz signal back onto the laser injection current (Vukičević *et al.* 2000) (**Figure 35**). The concept is similar to the one of optoelectronic oscillators as nonatomic systems (Yao and Maleki 1996). This setup requires a rigid structure and low loop delay times to reduce acceleration sensitivity, as changes in the RF phase are translated into frequency changes directly. Strekalov *et al.* (2006) demonstrated a fractional frequency instability of 5×10^{-10} at 1 s with this technique, when using a VCSEL and a 1-cm cell in zero magnetic field. One major problem with this setup is frequency tuning of the VCSEL as the RF power circulating in the loop varies.

Finally, a VCO can be inserted into the loop to modulate the laser (Vukičević *et al.* 2000). The 6.8-GHz signal detected on the photodetector can then be used to control the frequency of the VCO. Fractional frequency instabilities in the 10^{-11} range have been measured this way on the 0–0 transition in a centimeter-sized cell.

3.18.5.6 Ramsey-Type CPT Interrogation

In optically pumped clocks, narrower resonance lines can be achieved, when a (pulsed) Ramsey interrogation (Ramsey 1950, Thomas *et al.* 1982) is used rather than a continuous interrogation. Some of the first CPT resonances were measured in an atomic beam by using Ramsey-type interrogation. In a similar manner, a pulsed CPT clock has been proposed in a vapor cell (Zanon *et al.* 2005). The first pulse creates a ground-state coherence in the atoms followed by a precession in the dark. Coherence is then measured with a second pulse. One advantage of such a system is the reduction of power broadening. In the case of a pulsed technique, while continuous CPT resonances broaden linearly with light power, the width of the Ramsey fringes is given by the inverse time between pulses, e.g., the period during which the coherence precesses in the dark. Unfortunately, the decoherence time in a 1-mm cell is on the order of milliseconds.

3.18.5.7 N-Resonances

While CPT is a two-photon resonance, the so-called *N*-resonance is a three-photon process, which results in similar narrow lines (Phillips *et al.* 2005, Zibrov *et al.* 2005). **Figure 36(a)** shows a level diagram of this scheme. A two-photon resonance is created between the two ground states $|1\rangle$ and $|2\rangle$ by the two red-detuned light fields E_1 and E_2 if the Raman condition is fulfilled, i.e., the difference frequency between these two states is equal to the ground-state splitting frequency $\delta_R = \omega_1 - \omega_2 - \Delta_{HFS} = 0$. This condition is simultaneously probed by the field E_1 resonant with the transition $|2\rangle \rightarrow |3\rangle$. Off Raman resonance, E_1 pumps most of the atoms into the state $|1\rangle$. When tuned onto Raman resonance, however, atoms are pumped back into the state $|2\rangle$, increasing the absorption. This can be seen schematically in **Figure 36(b)**, where the transmission of E_1 is plotted as a function of Raman detuning. The experimental setup is fairly similar to the conventional CPT case with a laser modulated at the full hyperfine ground-state splitting frequency. The major difference is the use of a Fabry–Perot etalon to transmit only E_1 onto the detector in order to reach high resonance contrasts up to 30% (Phillips *et al.* 2005) (contrast is defined here as h_{Nres}/B_{GND}). It has been found that contrasts are higher on the D_2 line as compared to the D_1 line, the opposite of the case of CPT (Novikova *et al.* 2006a).

The shot noise in this system can be potentially lower than in the case of CPT, since the absorption is increased on resonance, and light shifts can be reduced in a way similar to that developed for CPT (Levi *et al.* 2000, Vanier *et al.* 1999, Zhu and Cutler 2000) by choosing a favorable modulation index (Novikova *et al.* 2006b).

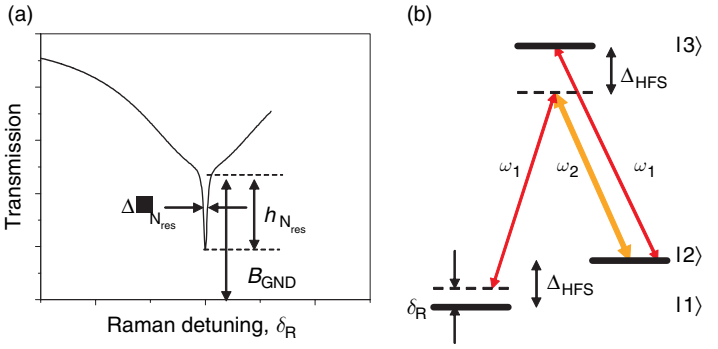

Figure 36 *N*-Resonance scheme. (a) Probe light transmission (ω_1) versus Raman detuning. (b) Three-level diagram showing probe (ω_1) and drive (ω_2) fields with their respective detunings.

3.18.5.8 Others

Recently, a miniature atomic clock was proposed in a solid-state system (White and Hajimiri 2005). The vanadium ion in magnesium oxide shows relatively narrow transitions around 1 MHz linewidth at 1.1 GHz. Such a solid-state atomic clock can be potentially very small and consumes very little power, with frequency instabilities around 10^{-8} to 10^{-9} at 1 s.

CPT spectroscopy is chosen as an all-optical interrogation technique in most approaches. One of the major arguments for this is the lack of a microwave cavity, which constrains the smallest possible size of the clock to a few centimeters. However, it has been shown that microwave resonances can nevertheless be seen in millimeter-sized cells without the use of a cavity, by the use of only small microwave power (Robinson 2003). **Figure 37(a)** shows a photograph of such a setup, where a 1-mm-diameter cell, made from an optical fiber with a CO_2 laser, is inside a copper microwave loop resonator. The magnetic RF field required to cause a clock transition can be roughly estimated to be 0.4 μT for a line of 3 kHz width. Creating this field in a current loop of 2 mm diameter would require roughly 0.6 mA of current, or 20 μW of power into 50 Ω. When using a tuned circuit cavity, the power could be reduced by the quality factor. Unloaded *Q*s around 200 seem possible with simple helical resonators like the one shown in **Figure 37(b)**. Even though these are only rough estimates, it can be seen that it does not necessarily require a high-*Q* large microwave cavity or a huge amount of power to excite a microwave clock resonance. One issue in such a lumped-parameter setup could arise from the stability of the microwave phase. The setup shown in **Figure 37** relies on the near-field and therefore has a decent confinement of the field over the dimension of the cell, but the setup nevertheless needs external shielding to ensure stability of the field.

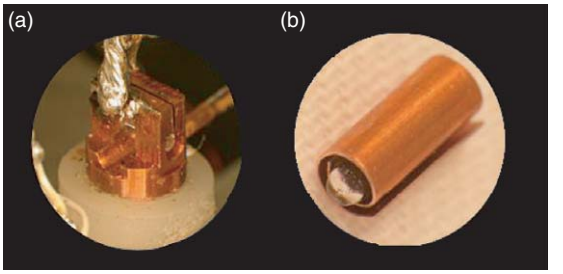

Figure 37 Photograph of a rubidium vapor cell of diameter 1 mm (a) inside a microwave loop and (b) inside a helical resonator (b) with a resonance frequency of 6.83 GHz and an unloaded *Q* of 200 (with and without cells).

3.18.6 Other MEMS Atomic Sensors

The technology discussed in this chapter is not limited to CSACs, but could rather open an avenue to a wide variety of chip-scale atomic sensors. Atomic and molecular transitions have proven useful in applications such as magnetometers (Allred *et al.* 2002, Bloom 1962), gyroscopes (Frazer 1963, Gustavson *et al.* 1997), accelerometers (Clauser 1988), gravimeters (Snadden *et al.* 1998), RF power meters (Camparo 1998b), and optical information storage (Fleischhauer and Lukin 2000, Liu *et al.* 2001). Furthermore, a stable frequency reference might be of value not only in the microwave regime, but in the optical regime as well. Stable optical wavelengths are used in devices such as interferometers, distance measurement, microscopy, and chemical trace detection. Combining wafer-level MEMS fabrication techniques with atomic stabilities and the ability to make absolute measurements without recalibration

could make these chip-scale atomic devices a viable technology for small, low-power applications.

Some chip-scale sensors based on these microfabrication techniques have already been demonstrated already. Two chip-scale atomic magnetometers (CSAMs) were constructed similar to the CASC physics package shown in **Figure 8**. One of them used CPT interrogation on a magnetically sensitive hyperfine transition (Schwindt *et al.* 2004) and reached a sensitivity of 50 pT $Hz^{-1/2}$ at 10 Hz in a 12-mm^3 package consuming 195 mW power. The so-called Mx magnetometer was based on the alignment of atoms in a magnetic field (Aleksandrov *et al.* 1995, Gröger *et al.* 2006). The precession frequency of the atoms was then used as a direct measure of the total magnetic field. The sensitivity was 6 pT $Hz^{-1/2}$ between 1 and 100 Hz bandwidth (Schwindt *et al.* 2006).

Furthermore, a microfabricated saturated absorption spectroscopy (Hänsch *et al.* 1971, Letokhov 1976) setup was demonstrated as an example of an optical wavelength reference with a MEMS cell and miniature optical components (**Figure 38**) (Knappe *et al.* 2006). It shows sub-Doppler linewidths on the order of 25 MHz at 795 nm optical wavelength and could be used to stabilize a diode laser to this transition. Frequency stabilities similar to those in table-top setups are expected.

These are just two examples of applications where microfabricated alkali cells are used in atomic sensors. While alkali atoms are often favored for spectroscopic applications, due to their relatively low vapor pressure and favorable transition frequencies, the technology introduced here is not necessarily limited to alkali atoms. We therefore expect chip-scale atomic devices to find applications in a wide variety of areas where size, cost, and power consumption need to be combined with high precision.

Acknowledgments

I thank John Kitching, Hugh Robinson, Zoya Popović, Leo Hollberg, and Robert Wynands for extensive reading of this manuscript as well as for their helpful and critical suggestions. Alan Brannon and Vishal Shah contributed through useful discussions.

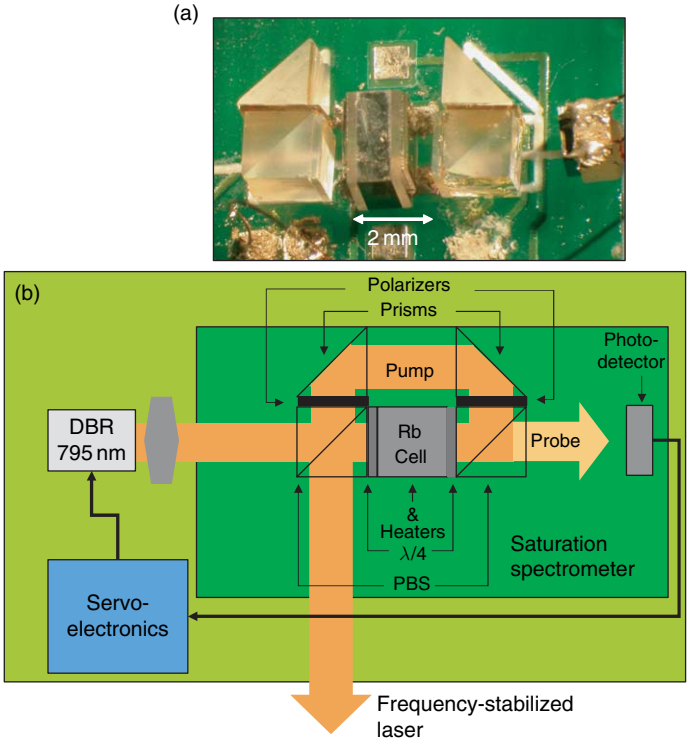

Figure 38 (a) Photograph of a microfabricated saturated absorption spectrometer setup. (b) Schematic of the microfabricated setup (dark green), which consists of a vapor cell with two heaters, two polarizing beamsplitters, two polarizers, two prisms, two quarter waveplates, and a photodetector. The light green shows a schematic of a stable wavelength reference including a laser locked to a stable sub-Doppler absorption resonance.

Commercial Rb standards: See, for example, Symmetricom X-72 Precision Rubidium Oscillator, Stanford Research Systems PRS10 Rubidium Frequency Standard, Accubeat AR-100B Rubidium Frequency Standard, Frequency Electronics FE-5658A Rubidium Atomic Frequency Standard, Temex LCR-900 Low Cost Rubidium; references are for technical clarity and do not imply endorsement by NIST.

References

Affolderbach C, Nagel A, Knappe S, Jung C, Wiedenmann D, Wynands R 2000 Nonlinear spectroscopy with a vertical-cavity surface-emitting laser (VCSEL). *Appl. Phys. B Lasers Opt.* **70**, 407–13

Affolderbach C, Knappe S, Wynands R, Taichenachev A V, Yudin V I 2002 Electromagnetically induced transparency and absorption in a standing wave. *Phys. Rev. A* **65**, 043810

Affolderbach C, Droz F, Mileti G 2006 Experimental demonstration of a compact and high-performance laser-pumped rubidium gas cell atomic frequency standard. *IEEE Trans. Instrum. Meas.* **55**, 429–35

Aleksandrov E B, Balabas M V, Vershovski A K, Ivanov A E, Yakobson N N, Velichanski V L, Senkov N V 1995 Laser pumping in the scheme of an Mx-magnetometer. *Opt. Spectrosc.* **78**, 325–32

Alexandrov E B, Balabas M V, Budker D, English D, Kimball D F, Li C H, Yashchuk V V 2002 Light-induced desorption of alkali-metal atoms from paraffin coating. *Phys. Rev. A* **66**, 042903

Allan D W 1987 Time and frequency (time-domain) characterization, estimation, and prediction of precision clocks and oscillators. *IEEE Trans. UFFC* **34**, 647–54

Allard N, Kielkopf J 1982 The effect of neutral nonresonant collisions on atomic spectral lines. *Rev. Mod. Phys.* **54**, 1103–82

Allred J C, Lyman R N, Kornack T W, Romalis M V 2002 High-sensitivity atomic magnetometer unaffected by spin-exchange relaxation. *Phys. Rev. Lett.* **89**, 130801

Alzetta G, Gozzini A, Moi L, Orriols G 1976 Experimental-method for observation of Rf transitions and laser beat resonances in oriented Na vapor. *Nuovo Cim.* **36**, 5–20

Alzetta G, Botti L, Cartaleva S, Celli R M, Rossi A 1999 Superposition of states and quantum interference in rubidium by diode laser modulation. *Proceedings of SPIE – 10th International Society for Optical Engineering,* Varna, Bulgaria, pp. 195–9

Arditi M, Carver T R 1961 Pressure, light, and temperature shifts in optical detection of 0-0 hyperfine resonance of alkali metals. *Phys. Rev.* **124**, 800–9

Arimondo E 1996a Coherent population trapping in laser spectroscopy.: In: Wolf E (ed.) p. *Progress in Optics. Elsevier Science Publication B V, Amsterdam, The Netherlands, Vol. 35*

Arimondo E 1996b Relaxation processes in coherent-population trapping. *Phys. Rev. A* **54**, 2216–23

Arimondo E, Orriols G 1976 Non-absorbing atomic coherences by coherent 2-photon transitions in a 3-level optical-pumping. *Lett. Nuovo Cim.* **17**, 333–8

Aspect A, Arimondo E, Kaiser R, Vansteenkiste N, Cohentannoudji C 1988 Laser cooling below the one-photon recoil energy by velocity-selective coherent population trapping. *Phys. Rev. Lett.* **61**, 826–9

Avalon Photonics, Avalon Photonics Datacom VCSELs, http://www.avap.ch

Balabas M V, Budker D, Kitching J, Schwindt P D D, Stalnaker J E 2006 Magnetometry with millimeter-scale antirelaxation-coated alkali-metal vapor cells. *J. Opt. Soc. Am. B* **23**, 1001–6

Barrat J P, Cohen-Tannoudji C 1961 Etude du pompage optique dans le formalisme de la matrice densité. *J. Phys. Radium* **22**, 329–36

Bentley C L Jr., Liu J 1999 LWI in a driven lambda three-level atom and effects of the probe laser on EIT. *Opt. Commun.* **169**, 289–99

Beverini N, Minguzzi P, Strumia F 1971 Foreign-gas-induced cesium hyperfine relaxation. *Phys. Rev. A* **4**, 550–5

Beverini N, Strumia F, Rovera G 1981 Buffer gas-pressure shift in the $M_f = 0 - M_f = 0$ ground-state hyperfine line in Cs. *Opt. Commun.* **37**, 394–6

Bhaskar N D 1995 Potential for improving the rubidium frequency standard with a novel optical pumping scheme using diode lasers. *IEEE Trans. UFFC* **42**, 15–20

Bloch M, Pascaru I, Stone C, Mcclelland T 1993 Subminiature rubidium frequency standard for commercial applications. *IEEE International Frequency Control Symposium,* Salt Lake City, UT, USA, pp. 164–77

Bloch M, Mancini O, Mcclelland T 2000 Performance of rubidium and quartz clocks in space. *2000 IEEE Frequency Control Symposium,* Kansas City, MO, USA, pp. 505–9

Bloembergen N, Purcell E M, Pound R V 1948 Relaxation effects in nuclear magnetic resonance absorption. *Phys. Rev.* **73**, 679–712

Bloom A L 1962 Principles of operation of the rubidium vapor magnetometer. *Appl. Opt.* **1**, 61–8

Bouchiat M A, Brossel J 1966 Relaxation of optically pumped Rb atoms on paraffin-coated walls. *Phys. Rev.* **147**, 41–54

Brandt S, Nagel A, Wynands R, Meschede D 1997 Buffer-gas-induced linewidth reduction of coherent dark resonances to below 50 Hz. *Phys. Rev. A* **56**, R1063–66

Brannon A, Breitbarth J, Popović Z 2005 A low-power, low phase noise local oscillator for chip-scale atomic clocks. *2005 IEEE MTT-S International Microwave Symposium,* Long Beach, CA, pp. 1535–8

Brannon A, Breitbarth J, Janković M, Popović Z 2006a Low-power, low phase noise local oscillators for chip-scale atomic clocks. *IEEE Trans. MTT-S,* submitted

Brannon A, Janković M, Breitbarth J, Popović Z, Gerginov V, Shah V, Knappe S, Hollberg L, Kitching J 2006b A local oscillator for chip-scale atomic clocks at NIST. *IEEE Frequency Control Symposium,* Miami, FL, USA, pp. 443–7

Buckle S J, Barnett S M, Knight P L, Lauder M A, Pegg D T 1986 Atomic interferometers – Phase-dependence in multilevel atomic transitions. *Opt. Acta* **33**, 1129–40

Budker D, Hollberg L, Kimball D F, Kitching J, Pustelny S, Yashchuk V V 2005 Microwave transitions and nonlinear magneto-optical rotation in anti-relaxation-coated cells. *Phys. Rev. A* **71**, 012903

Camparo J C 1998a Conversion of laser phase noise to amplitude noise in an optically thick vapor. *J. Opt. Soc. Am. B* **15**, 1177–86

Camparo J C 1998b Atomic stabilization of electromagnetic field strength using Rabi resonances. *Phys. Rev. Lett.* **80**, 222–5

Camparo J 2004 Frequency equilibration and the light-shift effect for block IIR GPS rubidium clocks. *Precise Time and Time Interval (PTTI) Meeting,* Washington, DC, USA

Camparo J C, Buell W F 1997 Laser PM to AM conversion in atomic vapors and short term clock stability. *IEEE Frequency Control Symposium*, Orlando, FL, USA, pp. 253–8

Camparo J C, Frueholz R P, Volk C H 1983 Inhomogeneous light shift in alkali-metal atoms. *Phys. Rev. A* **27**, 1914–24

Camparo J C, Klimcak C M, Herbulock S J 2005 Frequency equilibration in the vapor-cell atomic clock. *IEEE Trans. Instrum. Meas.* **54**, 1873–80

Chang-Hasnain C J, Harbison J P, Hasnain G, Von Lehmen A C, Florez L T, Stoffel N G 1991 Dynamic, polarization, and transverse mode characteristics of vertical cavity surface emitting lasers. *IEEE J. Quantum Electron.* **27**, 1402–9

Chantry P J, Liberman I, Verbanets W R, Petronio C F, Cather R L, Partlow W D 1996 Miniature laser-pumped cesium cell atomic clock oscillator. *IEEE International Frequency Control Symposium,* Honolulu, HI, pp. 1002–10

Chavez-Pirson A, Ando H, Saito H, Kanbe H 1993 Polarization properties of a vertical cavity surface emitting laser using a fractional layer superlattice gain medium. *Appl. Phys. Lett.* **62**, 3082–4

Choquette K D, Leibenguth R E 1994 Control of vertical-cavity laser polarization with anisotropic transverse cavity geometries. *IEEE Photon. Technol. Lett.* **6**, 40–2

Choquette K D, Schneider R P Jr., Lear K L, Geib K M 1994 Low threshold voltage vertical-cavity lasers fabricated by selective oxidation. *Electron. Lett.* **30**, 2043–4

Clauser J F 1988 Ultrahigh sensitivity accelerometers and gyroscopes using neutral atom matter-wave interferometry. *Physica B and C* **151**, 262–72

Coffer J G, Anderson M, Camparo J C 2002 Collisional dephasing and the reduction of laser phase-noise to amplitude-noise conversion in a resonant atomic vapor. *Phys. Rev. A* **65**, 033807

Copley G, Krause L 1969 Trapping and quenching of potassium resonance radiation. *Can. J. Phys.* **47**, 533–9

Cyr N, Têtu M, Breton M 1993 All-optical microwave frequency standard – A proposal. *IEEE Trans. Instrum. Meas.* **42**, 640–9

Dalton B J, Knight P L 1982 The effects of laser field fluctuations on coherent population trapping. *J. Phys. B* **15**, 3997–4015

Darpa Mto Csac Project, http://www.darpa.mil/mto

Debernardi P, Gian Paolo B 2003 Coupled mode theory: A powerful tool for analyzing complex VCSELs and designing advanced device features. *IEEE J. Quantum Electron.* **9**, 905–17

Degen C, Fischer I, Elsäßer W, Fratta L, Debernardi P, Bava G P, Brunner M, Hävel R, Moser M, Gulden K 2001 Transverse modes in thermally detuned oxide-confined vertical-cavity surface-emitting lasers. *Phys. Rev. A* **63**, 023817

Di Sopra F M, Zappe H P, Moser M, Hovel R, Gauggel H P, Gulden K 1999 Near-infrared vertical-cavity surface-emitting lasers with 3-MHz linewidth. *IEEE Photon. Technol. Lett.* **11**, 1533–5

Dicke R H 1953 The effect of collisions upon the Doppler width of spectral lines. *Phys. Rev.* **89**, 472–3

Ekinci K L, Roukes M L 2005 Nanoelectromechanical systems. *Rev. Sci. Instrum.* **76**, 061101

Enloe L H, Rodda J L 1965 Laser phase-locked loop. *Proc. IEEE* **52**, 165–6

Erhard M, Nußmann S, Helm H 2000 Power broadening and Doppler effects of coherent dark resonances in Rb. *Phys. Rev. A* **62**, 061802

Erklund E J, Shkel A M 2007 Glass blowing on wafer level. *J. Microelectromech. Syst.,* **16**, 232–9

Espe W 1966 *Materials of High Vacuum Technology*. Pergamon, Oxford

Fleischhauer M, Lukin M D 2000 Dark-state polaritons in electromagnetically induced transparency. *Phys. Rev. Lett.* **84**, 5094–7

Fleischhauer M, Imamoglu A, Marangos J P 2005 Electromagnetically induced transparency: Optics in coherent media. *Rev. Mod. Phys.* **77**, 633–73

Frazer J T 1963 Optically pumped magnetic resonance gyroscope and direction sensor. *US PTO* 3(103) 621

Fruehauf H 2001 Fast ''direct-P(Y)'' GPS signal acquisition using a special portable clock. *33rd Annual Precise Time and Time Interval (PTTI) Meeting,* Long Beach, CA, USA, pp. 359–69

Frueholz R P, Volk C H, Camparo J C 1983 Use of wall coated cells in atomic frequency standards. *J. Appl. Phys.* **54**, 5613–17

Fumio K, Susumu K, Kenichi I 1989 Room-temperature continuous wave lasing characteristics of a GaAs vertical cavity surface-emitting laser. *Appl. Phys. Lett.* **55**, 221–2

Gerginov V, Knappe S, Schwindt P D D, Shah V, Liew L, Moreland J, Robinson H G, Hollberg L, Kitching J, Brannon A, Breitbarth J, Popovic Z 2005 Component-level demonstration of a microfabricated atomic frequency reference. *Proceedings of the 2005 IEEE International Frequency Control Symposium and Exposition,* Vancouver, Canada, pp. 758–66

Gerginov V, Knappe S, Shah V, Schwindt P D D, Hollberg L, Kitching J 2006 Long-term frequency instability of atomic frequency references based on coherent population trapping and microfabricated vapor cells. *J. Opt. Soc. Am. B* **23**, 593–7

Gerginov V, Knappe S, Shah V, Hollberg L, Kitching J 2007 Laser noise cancellation in single-cell CPT clocks. *Rev. Sci. Instrum.,* accepted

Gierkink S L J, Levantino S, Frye R C, Samori C, Boccuzzi V 2003 A low-phase-noise 5-GHz CMOS quadrature VCO using superharmonic coupling. *IEEE J. Solid-State Circ.* **38**, 1148–54

Godone A, Levi F, Micalizio S, Vanier J 2000 Theory of the coherent population trapping maser: A strong-field self-consistent approach. *Phys. Rev. A* **62**, 053402

Godone A, Levi F, Micalizio S, Vanier J 2002 Dark-line in optically-thick vapors: Inversion phenomena and line width narrowing. *Eur. Phys. J. D* **18**, 5–13

Gong F, Jau Y Y, Jensen K, Happer W 2006 Electrolytic fabrication of atomic clock cells. *Rev. Sci. Instrum.* **77**, 076101

Grabherr M, Jager R, Michalzik R, Weigl B, Reiner G, Ebeling K J 1997 Efficient single-mode oxide-confined GaAs VCSEL's emitting in the 850-nm wavelength regime. *IEEE Photon. Technol. Lett.* **9**, 1304–6

Gray H R, Whitley R M, Stroud C R Jr. 1978 Coherent trapping of atomic populations. *Opt. Lett.* **3**, 218–20

Gröger S, Bison G, Schenker J L, Wynands R, Weis A 2006 A high-sensitivity laser-pumped Mx magnetometer. *Eur. Phys. J. D* **38**, 239–47

Guo H, Lal A 2003 Self-powered photon source. *12th Int. Conf. Solid State Sensors, Actuators and Microsystems (Transducers '03),* Boston, MA, USA, pp. 1474–7

Gustavson T L, Bouyer P, Kasevich M A 1997 Precision rotation measurements with an atom interferometer gyroscope. *Phys. Rev. Lett.* **78**, 2046–9

Häensch T W, Levenson M D, Schawlow A L 1971 Complete hyperfine structure of a molecular iodine line. *Phys. Rev. Lett.* **26**, 946–9

Happer W 1972 Optical pumping. *Rev. Mod. Phys.* **44**, 169–249

Harris S E 1997 Electromagnetically induced transparency. *Phys. Today* **50**, 36–42

Harris S E, Field J E, Imamoglu A 1990 Nonlinear optical processes using electromagnetically induced transparency. *Phys. Rev. Lett.* **64**, 1107–10

Hemmer P R, Ezekiel S, Leiby C C 1983 Stabilization of a microwave-oscillator using a resonance Raman transition in a sodium beam. *Opt. Lett.* **8**, 440–2

Hemmer P R, Shahriar M S, Lamelarivera H, Smith S P, Bernacki B E, Ezekiel S 1993 Semiconductor-laser excitation of Ramsey fringes by using a Raman transition in a cesium atomic-beam. *J. Opt. Soc. Am. B* **10**, 1326–9

Hemmer P R, Katz D P, Donoghue J, Croningolomb M, Shahriar M S, Kumar P 1995 Efficient low-intensity optical-phase conjugation based on coherent population trapping in sodium. *Opt. Lett.* **20**, 982–4

Ho J, Pascaru I, Stone C, Mcclelland T 1998 New Rubidium frequency standard designs for telecommunications applications. *IEEE International Frequency Control Symposium,* Pasadena, CA, USA, pp. 80–3

Hsu W-T, Nguyen C T C 2002 Stiffness-compensated temperature-insensitive micromechanical resonators. *15th IEEE Int. Conf. Micro Electro Mech. Syst.,* Las Vegas, NV, USA, pp. 731–4

Huffaker D L, Shin J, Deppe D G 1994 Low threshold half-wave vertical-cavity lasers. *Electron. Lett.* **30**, 1946–7

Ivanov E N, Tobar M E 2006 Low phase-noise microwave oscillators with interferometric signal processing. *IEEE Trans MTT-S* **54**, 3284–94

Ivanov E N, Tobar M E, Woode R A 1998 Microwave interferometry: Application to precision measurements and noise reduction techniques. *IEEE Trans. UFFC* **45**, 1526–36

Jau Y Y, Post A B, Kuzma N N, Braun A M, Romalis M V, Happer W 2003 The physics of miniature atomic clocks: 0–0 versus ''end'' resonances. *Proceedings of the Annual IEEE International Frequency Control Symposium,* Tampa, FL, pp. 33–6

Jau Y Y, Miron E, Post A B, Kuzma N N, Happer W 2004a Push-pull optical pumping of pure superposition states. *Phys. Rev. Lett.* **93**, 160802

Jau Y Y, Post A B, Kuzma N N, Braun A M, Romalis M V, Happer W 2004b Intense, narrow atomic-clock resonances. *Phys. Rev. Lett.* **92**, 110801

Jau Y Y, Post A, Gong F, Miron E, Kuzma N N, Happer W 2006 Physics and cell manufacturing of miniature atomic clocks. *NICT CSAC Workshop,* Tokyo, Japan

Jewell J L, Scherer A, Mccall S L, Lee Y H, Walker S, Harbison J P, Florez L T 1989 Low-threshold electrically pumped vertical-cavity surface-emitting microlasers. *Electron. Lett.* **25**, 1123–4

Jung C, Jager R, Grabherr M, Schnitzer P, Michalzik R, Weigl B, Muller S, Ebeling K J 1997 4.8 mW singlemode oxide confined top-surface emitting vertical-cavity laser diodes. *Electron. Lett.* **33**, 1790–1

Kaiser J, Degen C, Elsässer W 2002 Polarization-switching influence on the intensity noise of vertical-cavity surface-emitting lasers. *J. Opt. Soc. Am. B* **19**, 672–7

Kargapoltsev S V, Kitching J, Hollberg L, Taichenachev A V, Velichansky V L, Yudin V I 2004 High-contrast dark resonance in sigma(+)–sigma(−) optical field. *Laser Phys. Lett.* **1**, 495–9

Kasapi A, Jain M, Yin G Y, Harris S E 1995 Electromagnetically induced transparency: Propagation dynamics. *Phys. Rev. Lett.* **74**, 2447–50

Kazakov G, Matisov B, Mazets I, Mileti G 2005a Optimized scheme of a rubidium all-optical frequency standard. *Tech. Phys. Lett.* **31**, 1009–10

Kazakov G, Matisov B, Mazets I, Mileti G, Delporte J 2005b Pseudoresonance mechanism of all-optical frequency-standard operation. *Phys. Rev. A* **72**, 063408

Khanna A P S, Gane E, Chong T 2003 A 2GHz voltage tunable FBAR oscillator. *IEEE MTT-S International Microwave Symposium*, Philadelphia, PA, pp. 717–20

Kibble B P, Copley G, Krause L 1967 Effect of imprisonment of radiation in sodium vapor on the measured lifetime of the $3\,^2P$ States. *Phys. Rev.* **153**, 9–12

King R, Wiedenmann D, Schnitzer P, Jaeger R, Michalzik R, Ebeling K J 1998 Single-mode and multimode 2D VCSEL arrays for parallel optical interconnects. *Conference Digest – IEEE International Semiconductor Laser Conference,* Nara, Japan, pp, 103–4

Kitching J 2003 *Local oscillator requirements for chip-scale atomic clocks. Unpublished*

Kitching J, Hollberg L, Knappe S, Wynands R 2001a Compact atomic clock based on coherent population trapping. *Electron. Lett.* **37**, 1449–51

Kitching J, Hollberg L, Knappe S, Wynands R 2001b Frequency-dependent optical pumping in atomic Λ-systems. *Opt. Lett.* **26**, 1507–9

Kitching J, Robinson H G, Hollberg L, Knappe S, Wynands R 2001c Optical-pumping noise in laser-pumped, all-optical microwave frequency references. *J. Opt. Soc. Am. B* **18**, 1676–83

Kitching J, Knappe S, Hollberg L 2002 Miniature vapor-cell atomic-frequency references. *Appl. Phys. Lett.* **81**, 553–5

Kitching J, Knappe S, Schwindt P D D, Shah V, Hollberg L, Liew L, Moreland J 2004 Power dissipation in vertically integrated chip-scale atomic clocks. *Proceedings of the 2004 IEEE International Frequency Control Symposium,* Montreal, Canada, pp. 781–4

Kleppner D, Goldenberg H M, Ramsey N F 1962 Theory of the hydrogen maser. *Phys. Rev.* **126**, 603–15

Knappe S 2001 Dark resonance magnetometers and atomic clocks. *Ph.D. Thesis*, University of Bonn

Knappe S, Kemp W, Affolderbach C, Nagel A, Wynands R 1999 Splitting of coherent population-trapping resonances by the nuclear magnetic moment. *Phys. Rev. A* **61**, 012508

Knappe S, Wynands R, Kitching J, Robinson H G, Hollberg L 2001 Characterization of coherent population-trapping resonances as atomic frequency references. *J. Opt. Soc. Am. B* **18**, 1545–53

Knappe S, Kitching J, Hollberg L, Wynands R 2002 Temperature dependence of coherent population trapping resonances. *Appl. Phys. B Lasers Opt.* **74**, 217–22

Knappe S, Velichansky V, Robinson H G, Kitching J, Hollberg L 2003a Compact atomic vapor cells fabricated by laser-induced heating of hollow-core glass fibers. *Rev. Sci. Instrum.* **74**, 3142–5

Knappe S, Velichansky V, Robinson H G, Liew L, Moreland J, Kitching J, Hollberg L 2003b Atomic vapor cells for miniature frequency references. *Proceedings of the 2003 IEEE International Frequency Control Symposium and PDA Exhibition Jointly with the 17th European Frequency and Time Forum,* Tampa, FL, pp. 31–2

Knappe S, Hollberg L, Kitching J 2004a Dark-line atomic resonances in submillimeter structures. *Opt. Lett.* **29**, 388–90

Knappe S, Shah V, Schwindt P D D, Hollberg L, Kitching J, Liew L A, Moreland J 2004b A microfabricated atomic clock. *Appl. Phys. Lett.* **85**, 1460–2

Knappe S, Gerginov V, Schwindt P D D, Shah V, Robinson H, Hollberg L, Kitching J 2005a Atomic vapor cells for chip-scale atomic clocks with improved long-term frequency stability. *Opt. Lett.* **30**, 2351–3

Knappe S, Schwindt P D D, Shah V, Hollberg L, Kitching J, Liew L, Moreland J 2005b A chip-scale atomic clock based on Rb-87 with improved frequency stability. *Opt. Expr.* **13**, 1249–53

Knappe S, Robinson H G, Hollberg L 2007 Microfabricated saturated absorption laser spectrometer. *Optics Express* **15**, 6293–9

Kocharovskaya O 1992 Amplification and lasing without inversion. *Phys. Rep.* **219**, 175–90

Korsunsky E A, Leinfellner N, Huss A, Baluschev S, Windholz L 1999 Phase-dependent electromagnetically induced transparency. *Phys. Rev. A* **59**, 2302–5

Kosachiov D, Matisov B, Rozhdestvensky Y 1991 Coherent population trapping – Sensitivity of an atomic system to the relative phase of exciting fields. *Opt. Commun.* **85**, 209–12

Kosachiov D V, Matisov B G, Rozhdestvensky Y V 1992 Coherent phenomena in multilevel systems with closed interaction contour. *J. Phys. B* **25**, 2473–88

Koyama Y, Matsura H, Atsumi K, Nakamuta K, Sakai M, Maruyama I 2000 An ultra-miniature rubidium frequency standard. *IEEE International Frequency Control Symposium,* Kansas City, MO, pp. 694–9

Kubena R L, Stratton F P, Chang D T, Joyce R J, Hsu T Y, Lim M K, M'closkey R T 2005 MEMS-based quartz oscillators and filters for on-chip integration. *Proceedings of the 2005 IEEE International Frequency Control Symposium and Exposition,* Vancouver, Canada, pp. 122–7

Kusters J A, Adams C A 1999 Performance requirements of communication base station time standards. *RF Design* May 28–30, 1999

Kwakernaak M H, Lipp S, Mcbride S, Zanzucchi P, Chan W K, Khalfin V B, An H, Whaley J R D, Willner B I, Ulmer A, Li J Z, Davis T, Braun A M, Abeles J H, Post A, Jau Y-Y, Kuzma N N, Happer W 2004 Components for batch-fabricated chip-scale atomic clock. *Technical Digest of 36th Annual Precise Time and Time Interval (PTTI) Meeting,* Washington, DC, USA, pp. 355

Lai S L, Ramanath G, Allen L H, Infante P, Ma Z 1995 High-speed ($10^{4\circ}$C/s) scanning microcalorimetry with monolayer sensitivity (J/m^2). *Appl. Phys. Lett.* **67**, 1229–31

Larsson A, Carlsson C, Gustavsson J, Haglund A, Modh P, Bengtsson J 2004 *Direct high-frequency modulation of VCSELs and applications in fibre optic RF and microwave links*. New J. Phys. **6**, 176. http://www.njp.org/

Laws A, Chang R Y J, Bright V M, Lee Y C 2005 Thermal management for chip-scale atomic clocks. *Proc. ASME/ Pacific Rim Tech. Conf. Exhibit. Integration and Packaging of MEMS, NEMS, and Electronic Systems: Advances in Electronic Packaging,* San Francisco, CA, 2005, pp. 741–6

Lear K L, Mar A, Choquette K D, Kilcoyne S P, Schneider R P Jr., Geib K M 1996 High-frequency modulation of oxide-confined vertical cavity surface emitting lasers. *Electron. Lett.* **32**, 457–8

Lee C, Guo H, Radhakrishnan S, Lal A, Szekely C, Mcclelland T A, Pisano A 2004 A batch fabricated rubidium-vapor resonance cell for chip scale atomic clock. *Solid State Sensor and Actuator Workshop,* Hilton Head Island, SC, USA

Lee H J, Adams C S, Kasevich M, Chu S 1996 Raman cooling of atoms in an optical dipole trap. *Phys. Rev. Lett.* **76**, 2658–61

Lee S, Nguyen C T C 2004 Mechanically-coupled micromechanical resonator arrays for improved phase noise. *Proceedings of the 2004 IEEE International Frequency Control Symposium and Exposition,* Montreal, Canada, pp. 144–50

Letokhov V S 1976 Saturation spectroscopy. In: Shimoda K (ed.) *High-Resolution Laser Spectroscopy.* Springer-Verlag, New York

Levi F, Godone A, Novero C, Vanier J 1997 On the use of a modulated laser for hyperfine frequency excitation in passive frequency standards. *11th Annual European Frequency and Time Forum*, Neuchatel, Switzerland

Levi F, Godone A, Vanier J 2000 Light shift effect in the coherent population trapping cesium maser. *IEEE Trans. UFFC* **47**, 466–70

Li S-S, Lin Y-W, Xie Y, Ren Z, Nguyen C T C 2004 Micromechanical ''hollow-disk'' ring resonators. *17th IEEE Int. Conf. Micro Electro Mechanical Systems (MEMS),* Maastricht, Netherlands, pp. 821–4

Liew L A, Knappe S, Moreland J, Robinson H, Hollberg L, Kitching J 2004 Microfabricated alkali atom vapor cells. *Appl. Phys. Lett.* **84**, 2694–6

Liew L, Moreland J, Knappe S, Shah V, Schwindt P, Gerginov V, Kitching J, Hollberg L 2005 Microfabricated alkali atom vapor cells with in-situ heating for atomic-based sensors. *Proc. 3rd Int. Symp. Sensor Science,* Juelich, Germany, pp. 181–3

Liew L, Moreland J, Gerginov V 2006 Wafer-level fabrication and filling of cesium vapor cells for chip-scale atomic devices. *Proceedings of the 20th Eurosensors Conference,* Goteberg, Sweden, paper W1B-P2

Liew L-A, Moreland J, Gerginov V 2007 Water-level filling of microfabricated atomic vapour cells based on thin-film deposition and photolysis of cesium azide. *Appl. Phys. Lett.* **90**, 114106

Liu C, Dutton Z, Behroozi C H, Vestergaard Hau L 2001 Observation of coherent optical information storage in an atomic medium using halted light pulses. *Nature* **409**, 490–3

Lukin M D, Yelin S F, Fleischhauer M, Scully M O 1999 Quantum interference effects induced by interacting dark resonances. *Phys. Rev. A* **60**, 3225–8

Lutwak R, Emmons D, Riley W, Garvey R M 2002 The chip-scale atomic clock – Coherent population trapping vs. conventional interrogation. *34th Annual Precise Time and Time Interval (PTTI) Meeting,* Reston, VA, USA, pp. 539–50

Lutwak R, Emmons D, English T, Riley W, Duwel A, Varghese M, Serkland D K, Peake G M 2003 The chip-scale atomic clock – Recent development progress. *35th Annual Precise Time and Time Interval (PTTI) Meeting,* San Diego, CA, USA, pp. 1–12

Lutwak R, Deng J, Riley W, Varghese M, Leblanc J, Tepolt G, Mescher M, Serkland D K, Geib K M, Peake G M 2004 The chip-scale atomic clock – Low-power physics package. *36th Annual Precise Time and Time Interval (PTTI) Meeting,* Washington, DC, USA, pp. 1–14

Lutwak R, Vlitas P, Varghese M, Mescher M, Serkland D K, Peake G M 2005 The MAC – A miniature atomic clock. *Joint Meeting of the IEEE International Frequency Control Symposium and the Precise Time and Time Interval (PTTI) Systems and Applications Meeting,* Vancouver, BC, Canada, pp. 752–7

Lyons H 1950 The atomic clock – A universal standard for frequency and time. *Am. Scholar* **19**, 159–68

Maichen W, Gaggl R, Korsunsky E, Windholz L 1995 Observation of phase-dependent coherent population trapping in optically closed atomic systems. *Europhys. Lett.* **31**, 189–94

Maichen W, Renzoni F, Mazets I, Korsunsky E, Windholz L 1996 Transient coherent population trapping in a closed loop interaction scheme. *Phys. Rev. A* **53**, 3444–8

Marangos J P 1998 Topical review electromagnetically induced transparency. *J. Mod. Opt.* **45**, 471–503

Mathur B S, Tang H, Happer W 1968 Light shifts in the alkali atoms. *Phys. Rev.* **171**, 11–19

McClelland T, Pascaru I, Shtaerman I, Stone C, Szekely C, Zacharski J, Bhaskar N D 1995 Subminiature rubidium frequency standard: Manufacturability and performance results from production units. *IEEE International Frequency Control Symposium,* San Francisco, CA, pp. 39–52

McClelland T, Pascaru I, Shtaerman I, Stone C, Szekely C, Zacharski J, Bhaskar N D 1996 Subminiature rubidium frequency standard: Performance improvements. *IEEE International Frequency Control Symposium,* Honolulu, HI, pp. 1011–16

McClelland T, Ho J, Pascaru I, Stone C 1999 Rb frequency standard with expanded operating temperature range. *Joint Meeting of the European Frequency and Time Forum and the IEEE International Frequency Control Symposium,* Besancon, France, pp. 137–40

Merimaa M, Lindvall T, Tittonen I, Ikonen E 2003 All-optical atomic clock based on coherent population trapping in ^{85}Rb. *J. Opt. Soc. Am. B* **20**, 273–9

Mileti G, Jinquan D, Walls F L, Jennings D A, Drullinger R E 1998 Laser-pumped rubidium frequency standards: New analysis and progress. *IEEE J. Quantum Electron.* **34**, 233–7

Mourant J M, Imbornone J, Tewksbury T 2000 A low phase noise monolithic VCO in SiGe BiCMOS. *IEEE Radio Frequency Integrated Circuits (RFIC) Symposium,* Boston, MA, pp. 65–8

Mueller G, Mueller M, Wicht A, Rinkleff R H, Danzmann K 1997 Optical resonator with steep internal dispersion. *Phys. Rev. A* **56**, 2385–9

Mukaihara T, Koyama F, Iga K 1993 Engineered polarization control of GaAs/AlGaAs surface-emitting lasers by anisotropic stress from elliptical etched substrate hole. *IEEE Photon. Technol. Lett.* **5**, 133–5

Mukaihara T, Ohnoki N, Hayashi Y, Hatori N, Koyama F, Iga K 1995a Polarization control of vertical-cavity surface emitting lasers using a birefringent metal/dielectric polarizer loaded on top distributed Bragg reflector. *IEEE J. Quantum Electron.* **1**, 667–73

Mukaihara T, Ohnoki N, Hayashi Y, Hatori N, Koyama F, Iga K 1995b Excess intensity noise originated from polarization fluctuation in vertical-cavity surface-emitting lasers. *IEEE Photon. Technol. Lett.* **7**, 1113–15

Mukoyama N, Otama H, Kuwata Y, Nakayama H 2006 850 nm Single mode oxide-confined VCSEL. *NICT Workshop on Chip Scale Atomic Clock Status and Potentiality,* NICT Headquarters, Koganei, Tokyo, Japan

Murphy J, Skidmore T 1994 A low-cost atomic clock: impact on the national airspace and GNSS availability. *Proc. ION GPS-94; 7th Int. Meet. Satellite Division of the Institute of Navigation,* Salt Lake City, UT, USA, pp. 1329–36

Myatt C J, Newbury N R, Wieman C E 1993 Simplified atom trap by using direct microwave modulation of a diode laser. *Opt. Lett.* **18**, 649–51

Nagel A 1999 Precision spectroscopy of coherent dark states in thermal cesium vapor. *Ph.D. thesis*, University of Bonn

Nguyen C T C 2005 MEMS technology for timing and frequency control. *Proceedings of the 2005 IEEE International Frequency Control Symposium and Exposition,* Vancouver, Canada, pp. 1–11

Nguyen C T-C, Howe R T 1993 Microresonator frequency control and stabilization using an integrated micro oven. *Dig. Tech. Pap., 7th Int. Conf. Solid-State Sensors and Actuators (Transducers '93),* Yokohama, Japan, pp. 1040–3

Nikonov D E, Rathe U W, Scully M O, Zhu S Y, Fry E S, Li X F, Padmabandu G G, Fleischhauer M 1994 Atomic coherence effects within the sodium D(1) manifold .2. Coherent optical-pumping. *Quantum Opt.* **6**, 245–60

Novikova I, Phillips D F, Zibrov A S, Walsworth R L, Taichenachev A V, Yudin V I 2006a *N*-resonances for D-1 and D-2 transitions. *Opt. Lett.* **31**, 2353–5

Novikova I, Phillips D F, Zibrov A S, Walsworth R L, Taichenachev A V, Yudin V I 2006b Cancellation of light shifts in an *N*-resonance clock. *Opt. Lett.* **31**, 622–4

Numai T, Kurihara K, Kuhn K, Kosaka H, Ogura I, Kajita M, Saito H, Kasahara K 1995 Control of light-output polarization for surface-emitting-laser type device by strained active layer grown on misoriented substrate. *IEEE J. Quantum Electron.* **31**, 636–42

Orriols G 1979 Non-absorption resonances by non-linear coherent effects in a 3-level system. *Nuovo Cim.* **53**, 1–24

Ostermann J M, Debernardi P, Jalics C, Michalzik R 2005 Polarization-stable oxide-confined VCSELs with enhanced single-mode output power via monolithically integrated inverted grating reliefs. *IEEE J. Quantum Electron.* **11**, 982–9

Pang W, Hongyu Y, Hao Z, Eun Sok K 2005 Electrically tunable and temperature compensated FBAR. *IEEE MTT-S International Microwave Symposium Digest,* Long Beach, CA, pp. 1279–82

Phillips D F, Fleischhauer A, Mair A, Walsworth R L, Lukin M D 2001 Storage of light in atomic vapor. *Phys. Rev. Lett.* **86**, 783–6

Phillips D F, Novikova I, Zibrov S, Smallwood C, Taichenachev A V, Yudin V I, Walsworth R L, Zibrov A S 2005 A novel absorption resonance for atomic clocks. *Proceedings of the 2005 IEEE International Frequency Control Symposium and Exposition,* Vancouver, Canada, pp. 767–73

Phillips D F, Novikova I, Wang C, Walsworth R L, Crescimanno M 2006 Modulation-induced frequency shifts in a coherent-population-trapping-based atomic clock *J. Opt. Soc. Am. B* **22**, 305–10

Photonics U Reliability study, http://www.ulmphotonics.de/

Post A B, Jau Y Y, Kuzma N N, Happer W 2005 Amplitude-versus frequency-modulated pumping light for coherent population trapping resonances at high buffer-gas pressure. *Phys. Rev. A* **72**, 1–17

Pozar D M 2001 *Microwave and RF Design of Wireless Systems*. John Wiley and Sons Inc., New York

Quinn T, (ed.) (2005) Special issue: Fifty years of atomic time-keeping: 1995 to 2005. *Metrologia*, **42**

Radhakrishnan S, Lal A 2005 Alkali metal-wax micropackets for chip-scale atomic clocks. *Dig. Tech. Pap. – Int. Conf. Solid State Sensors and Actuators and Microsystems, Transducers '05,* Seoul, Korea, pp 23–6

Ramsey N F 1950 A molecular beam resonance method with separated oscillating fields. *Phys. Rev.* **78**, 695–9

Risley A, Jarvis S Jr., Vanier J 1980 The dependence of frequency upon microwave power of wall-coated and buffer-gas-filled gas cell ^{87}Rb frequency standards. *J. Appl. Phys.* **51**, 4571–6

Robinson H G 2003 Personal communications

Robinson H, Ensberg E, Dehmelt H 1958 Preservation of spin state in free atom inert surface collisions. *Bull. Am. Phys. Soc.* **3**, 9

Robinson H G, Johnson C E 1982 Narrow ^{87}Rb hyperfine-structure resonances in an evacuated wall-coated cell. *Appl. Phys. Lett.* **40**, 771–3

Rochat P, Leuenberger B, Stehlin X 2002 A new synchronized ultra miniature rubidium oscillator. *IEEE Int. Freq. Contr. Symp,* New Orleans, LA, USA, pp. 451–4

Römisch S, Lutwak R 2006 Low-Power, 4.6-GHz stable oscillator for CSAC. *International Frequency Control Symposium,* Miami, FL, USA, pp. 448–51

Rosenbluh M, Shah V, Knappe S, Kitching J 2006 Differentially detected coherent population trapping resonances excited by orthogonally polarized laser fields. *Opt. Expr.* **14**, 6588–94

Ruther P, Herrscher M, Paul O 2004 A micro differential thermal analysis (/spl mu/DTA) system. *17th IEEE Int. Conf. Micro Electro Mechanical Systems (MEMS),* Maastricht, The Netherlands, pp. 165–8

Sargsyan A, Sarkisyan D, Papoyan A 2006 Dark-line atomic resonances in a submicron-thin Rb vapor layer. *Phys. Rev. A* **73**, 033803

Schmidt O, Wynands R, Hussein Z, Meschede D 1996 Steep dispersion and group velocity below c/3000 in coherent population trapping. *Phys. Rev. A* **53**, R27–30

Schmidt-Kaler F, Eschner J, Morigi G, Roos C F, Leibfried D, Mundt A, Blatt R 2001 Laser cooling with electromagnetically induced transparency: Application to trapped samples of ions or neutral atoms. *Appl. Phys. B* **73**, 807–14

Schwindt P D D, Knappe S, Shah V, Hollberg L, Kitching J, Liew L A, Moreland J 2004 Chip-scale atomic magnetometer. *Appl. Phys. Lett.* **85**, 6409–11

Schwindt P D D, Lindseth B, Knappe S, Shah V, Kitching J 2006 A chip-scale atomic magnetometer with improved sensitivity using the Mx technique. *Appl. Phys. Lett.,* **90**, 081102

Scully M O, Fleischhauer M 1992 High-sensitivity magnetometer based on index-enhanced media. *Phys. Rev. Lett.* **69**, 1360–3

Serkland D K, Peake G M, Geib K M, Lutwak R, Michael Garvey R, Varghese M, Mescher M 2006 VCSELs for atomic clocks. Chun Lei K D C (ed.) *Proceedings of SPIE – The International Society for Optical Engineering*, pp. 613208

Seurin J-F P, Chuang S L, Chirovski L M F, Choquette K D 2002 Novel VCSEL designs deliver high output power. *Laser Focus World* **38**, 119–24

Shah V, Knappe S, Hollberg L, Kitching J 2004 *On open Λ systems and the stability of coherent population trapping devices. Unpublished*

Shah V, Gerginov V, Schwindt P D D, Knappe S, Hollberg L, Kitching J 2006a Continuous light shift correction in modulated CPT clocks. *Appl. Phys. Lett.,* **89**, 151124

Shah V, Knappe S, Schwindt P D D, Gerginov V, Kitching J 2006b Compact phase delay technique for increasing the amplitude of coherent population trapping resonances in open Λ systems. *Opt. Lett.* **31**, 2335–7

Shahriar M S, Hemmer P R 1990 Direct excitation of microwave-spin dressed states using a laser-excited resonance Raman interaction. *Phys. Rev. Lett.* **65**, 1865–8

Shimuzi M, Mukaihara T, Koyama F, Iga K 1991 Polarisation control for surface emitting lasers. *Electron. Lett.* **27**, 1067–9

Simpson T B, Doft F, Golding W M 2003 Using laser diode instabilities for chip-scale stable frequency references. *Precise Time and Time Interval (PTTI) Meeting,* San Diego, CA, USA

Snadden M J, Mcguirk J M, Bouyer P, Haritos K G, Kasevich M A 1998 Measurement of the earth's gravity gradient with an atom interferometer-based gravity gradiometer. *Phys. Rev. Lett.* **81**, 971–4

Stähler M, Wynands R, Knappe S, Kitching J, Hollberg L, Taichenachev A, Yudin V 2002 Coherent population trapping resonances in thermal Rb-85 vapor: D-1 versus D-2 line excitation. *Opt. Lett.* **27**, 1472–4

Steck D 2003 A cesium D line data, http://steck.us/alkalidata

Steck D 2003 A Rubidium 87 D line data, http://steck.us/alkalidata

Stratton F P, Chang D T, Kirby D J, Joyce R J, Tsung-Yuan H, Kubena R L, Yook-Kong Y 2004 A MEMS-based quartz resonator technology for GHz applications. *Proceedings of the 2004 IEEE International Frequency Control Symposium and Exposition,* Montreal, Canada, 2004, pp. 27–34

Strekalov D, Matsko A B, Yu N, Savchenkov A, Maleki L 2006 Application of vertical cavity surface emitting lasers in self-oscillating atomic clocks. *J. Mod. Opt.*, **53**, 2469–84

Sturza M A 1984 GPS navigation using three satellites and a precise clock. *Global Positioning System*. Institute of Navigation, Washington, DC

Suzuki K, Abe Y, Ishihara N, Kudoh H, Fukugawa S 1998 Small-sized Rubidium oscillator. *IEEE International Frequency Control Symposium,* Pasadena, CA, USA, pp. 73–9

Taichenachev A V, Yudin V I, Velichansky V L, Kargapoltsev S V, Wynands R, Kitching J, Hollberg L 2004 High-contrast dark resonances on the D1 line of alkali metals in the field of counterpropagating waves. *JETP Lett.* **80**, 236–40

Taichenachev A V, Yudin V I, Velichansky V L, Zibrov S A 2005 On the unique possibility of significantly increasing the contrast of dark resonances on the D1 line of 87Rb. *JETP Lett.* **82**, 398–403

Tench R E, Peuse B W, Hemmer P R, Thomas J E, Ezekiel S, Leiby C C, Picard R H, Willis C R 1981 2 Laser raman difference technique applied to high-precision spectroscopy. *J. de Phys.* **42**, 45–51

Thomas J E, Hemmer P R, Ezekiel S, Leiby C C, Picard R H, Willis C R 1982 Observation of Ramsey fringes using a stimulated, resonance raman transition in a sodium atomic beam. *Phys. Rev. Lett.* **48**, 867–70

Townes C H 1951 Atomic clocks and frequency stabilization on microwave spectral lines. *J. Appl. Phys.* **22**, 1365–72

Vanier J 2001 Atomic frequency standard. *US PTO 6 320 472*

Vanier J 2005 Atomic clocks based on coherent population trapping: a review. *Appl. Phys. B Lasers Opt.* **81**, 421–42

Vanier J, Audoin C 1989 *The Quantum Physics of Atomic Frequency Standards*. Adam Hilger, Bristol

Vanier J, Audoin C 1992 *The Quantum Physics of Atomic Frequency Standards*. Adam Hilger, Bristol

Vanier J, Kunski R, Cyr N, Savard J Y, Têtu M 1982 On hyperfine frequency-shifts caused by buffer gases – Application to the optically pumped passive rubidium frequency standard. *J. Appl. Phys.* **53**, 5387–91

Vanier J, Godone A, Levi F 1998 Coherent population trapping in cesium: Dark lines and coherent microwave emission. *Phys. Rev. A* **58**, 2345–58

Vanier J, Godone A, Levi F 1999 Coherent microwave emission in coherent population trapping: Origin of the energy and of the quadratic light shift. *Proceedings of the Annual IEEE International Frequency Control Symposium,* Besancon, France, pp. 96–9

Vanier J, Godone A, Levi F, Micalizio S 2003a Atomic clocks based on coherent population trapping: Basic theoretical models and frequency stability. *Proceedings of the Annual IEEE International Frequency Control Symposium,* Tampa, FL, pp. 2–15

Vanier J, Levine M W, Janssen D, Delaney M 2003b Contrast and linewidth of the coherent population trapping transmission hyperfine resonance line in Rb-87: Effect of optical pumping. *Phys. Rev. A* **67**, 065801

Vanier J, Levine M W, Janssen D, Delaney M J 2003d The coherent population trapping passive frequency standard [Rb example]. *IEEE Trans. Instrum. Meas.* **52**, 258–62

Vanier J, Levine M W, Janssen D, Delaney M J 2003e On the use of intensity optical pumping and coherent population trapping techniques in the implementation of atomic frequency standards. *IEEE Trans. Instrum. Meas.* **52**, 822–31

Vanier J, Levine M, Kendig S, Janssen D, Everson C, Delany M 2004 Practical realization of a passive coherent population trapping frequency standard. *IEEE International Frequency Control Symposium,* Montreal, Canada, pp. 92–9

Vanier J, Levine M W, Kendig S, Janssen D, Everson C, Delaney M J 2005 Practical realization of a passive coherent population trapping frequency standard. *IEEE Trans. Instrum. Meas.* **54**, 2531–9

Vestergaard Hau L, Harris S E, Dutton Z, Behroozi C H 1999 Light speed reduction to 17 metres per second in an ultracold atomic gas. *Nature* **397**, 594–8

Vig J R Introduction to quartz frequency standard, SLCET-TR-92-1, http://www.ieee-uffc.org/freqcontrol/quartz/vig/vigtoc.htm

Vig J R 1993 Military applications of high accuracy frequency standards and clocks. *IEEE Trans. UFFC* **40**, 522–7

Vig J R, Yoonkee K 1999 Noise in microelectromechanical system resonators. *IEEE Trans. UFFC* **46**, 1558–65

Vukičević N, Zibrov A S, Hollberg L, Walls F L, Kitching J, Robinson H G 2000 Compact diode-laser based rubidium frequency reference. *IEEE Trans. UFFC* **47**, 1122–6

Walker T G, Happer W 1997 Spin-exchange optical pumping of noble-gas nuclei. *Rev. Mod. Phys.* **69**, 629–42

Wallis G, Pomerantz D 1969 Field assisted glass–metal sealing. *J. Appl. Phys.* **40**, 3946–9

Walls D F, Zoller P 1980 Coherent nonlinear mechanism for optical bistability from three level atoms. *Opt. Commun.* **34**, 260–4

Waltman S 2006 Frequency divider for a chip-scale atomic clock, Unpublished

Wang J, Butler J E, Hsu D S Y, Nguyen T C 2002 CVD polycrystalline diamond high-Q micromechanical resonators. *The 15th IEEE International Conference on Micro Electro Mechanical Systems,* Las Vegas, NV, USA, pp. 657–60

Wang Y-J, Eardley M, Knappe S, Moreland J, Hollberg L, Kitching J 2006 Magnetic resonance in an atomic vapor excited by a mechanical resonator. *Phys. Rev. Lett.* **97**, 227602

White C J, Hajimiri A H 2005 A solid-state atomic frequency standard. *Proceedings of the 2005 IEEE International Frequency Control Symposium and Exposition,* Vancouver, Canada, pp. 940–6

Whitley R M, Stroud C R 1976 Double optical resonance. *Phys. Rev. A* **14**, 1498–513

Wynands R, Nagel A 1999 Precision spectroscopy with coherent dark states. *Appl. Phys. B Lasers Opt.* **68**, 1–25

Yang G M, Macdougal M H, Dapkus P D 1995 Ultralow threshold current vertical-cavity surface-emitting lasers obtained with selective oxidation. *Electron. Lett.* **31**, 886–8

Yao X S, Maleki L 1996 Optoelectronic oscillator for photonic systems. *IEEE J. Quantum Electron.* **32**, 1141–9

Youngner D W, Detry J F, Zook J D 2005 MEMS frequency standard for devices such as atomic clocks. *US PTO 6 900 702 B2*

Zanon T, Guerandel S, De Clercq E, Holleville D, Dimarcq N, Clairon A 2005 High contrast Ramsey fringes with coherent-population-trapping pulses in a double lambda atomic system. *Phys. Rev. Lett.* **94**, 193002

Zhang H, Kim J, Pang W, Yu H, Kim E S 2005 5 5 GHz low-phase-noise oscillator based on FBAR with low TCF. *13th Int. Conf. Solid-State Sensors, Actuators and Microsystems, Dig. Tech. Pap. (Transducers '05),* Seoul, Korea, pp. 1100–1

Zhu M 2003 High contrast signal in a coherent population trapping based atomic frequency standard application. *IEEE International Frequency Control Symposium and PDA Exhibition Jointly with the 17th European Frequency and Time Forum,* Tampa, FL, USA, pp. 16–21

Zhu M 2004 Study of CPT in a vapor cell with optical phase locked diode lasers. *Proceedings of the John Hall Symposium,* Boulder, CO, USA, pp. 156–8

Zhu M, Cutler L S 2000 Theoretical and experimental study of light shift in a CPT-based Rb vapor cell frequency standard. *32nd Annual Precise Time and Time Interval (PTTI) Meeting,* Reston, VA, USA, pp. 311–24

Zhu M, Cutler L S 2001 Coherent population trapping-based frequency standard having a reduced magnitude of total a.c. stark shift. *US PTO 6 201 821*

Zibrov S, Novikova I, Phillips D F, Taichenachev A V, Yudin V I, Walsworth R L, Zibrov A S 2005 Three-photon-absorption resonance for all-optical atomic clocks. *Phys. Rev. A* **72**, 011801

Biography

Svenja Knappe received her diploma in Physics from the University of Bonn, Germany, in 1998. The topic for her diploma thesis was the investigation of single cesium atoms in a magneto-optical trap. She obtained her Ph.D. from the University of Bonn in 2001, with a thesis on "Dark resonance magnetometers and atomic clocks." Since 2001, she has been pursuing research in the Time and Frequency Division at NIST, Boulder, CO. Her research interests include precision laser spectroscopy, atomic clocks and atomic magnetometers, laser cooling, alkali vapor cell technology, applications of semiconductor lasers to problems in atomic physics and frequency control, and miniaturization of atomic spectroscopy.